Hindawi
Shock and Vibration
Volume 2018, Article ID 9430267, 17 pages
https://doi.org/10.1155/2018/9430267

Research Article

Dynamics Behavior Analysis of Parallel Mechanism with Joint Clearance and Flexible Links

Chen Xiulong,[1] **Jia Yonghao**,[1] **Deng Yu**,[1] **and Wang Qing**[2]

[1]*College of Mechanical and Electronic Engineering, Shandong University of Science and Technology, Qingdao 266590, China*
[2]*Institute of Nanoengineering, Shandong University of Science and Technology, Qingdao 266590, China*

Correspondence should be addressed to Chen Xiulong; cxldy99@163.com

Received 8 August 2017; Revised 26 December 2017; Accepted 28 January 2018; Published 4 March 2018

Academic Editor: Francesco Ripamonti

In this study, the dynamics behaviors analysis of parallel mechanism considering joint clearance and flexible links are investigated using a computational methodology. The nonlinear dynamic model of 4-UPS-RPS spatial parallel mechanism with clearance in spherical joint and flexible links is established by combining KED method and Lagrange method. The dynamic responses including collision force and motion characteristics of the moving platform are obtained. Chaos and bifurcation are analyzed. The effects of different clearances on the dynamics behaviors of the parallel mechanism are studied. The results show that 4-UPS-RPS spatial parallel mechanism is very sensitive to joint clearance and flexible links, and small variations in the clearance value can cause the mechanism change from periodic motion to chaotic motion. This research provides a methodology for forecasting the dynamics behavior of parallel mechanisms with clearance and flexible links.

1. Introduction

With the development of modern industry, the parallel mechanism is developing towards light weight, high speed, and high precision [1–3]. Because of the elastic deformation of the flexible components during the course of the movement and the nonlinear phenomenon existing in joint clearance caused by interaction, separation, and friction, the stability and the working accuracy of parallel mechanism can be greatly affected. Therefore, the dynamics behaviors analysis of parallel mechanism with joint clearance and flexible links must be taken into account.

At present, some scholars have made a series of achievements in the study of the elastic dynamics and the dynamics of mechanisms with clearance, respectively. Yu et al. [4] took the 3-RRR planar parallel mechanism as the research object, carried out the elastic dynamics modeling, and verified the validity of the theoretical analysis through experimental research. Lankararni and Nikravesh [5] proposed a nonlinear spring damping contact force model based on Hertz contact theory and coefficient of restitution and considered that material damping is the source of energy loss in the process of collision with a clearance mechanism. Flores and Ambrósio [6] analyzed the dynamic characteristics of slider crank mechanisms with clearances based on the L-N continuous contact model. Bai and Zhao [7] put forward a hybrid contact model with nonlinear stiffness coefficient and verified the correctness of the model. Bu et al. [8] proposed trajectory planning method based on the continuous contact model to avoid the separation of the elements of the joint with clearances. Dubowsky and Gardner [9] combined the perturbation coordinate method and the assumed mode method to establish the system motion equation and laid the theoretical foundation for considering both the subclearance and the flexible component. Zheng and Zhou [10] studied the effects of clearance values by ADAMS. Jin Chunmei and Qiu Yang [11] established the dynamic model of the elastic linkage mechanism with clearances based on the FMD theory and obtained the dynamic response of the elastic mechanism with clearances. Zhang et al. [12] built the dynamic model of the planar parallel mechanisms with multiple clearances and analyzed the effects of load, motion speed, and trajectory on the stability of the mechanism. Rahmanian and Ghazavi [13] illustrated the sensitivity of multibody mechanical systems

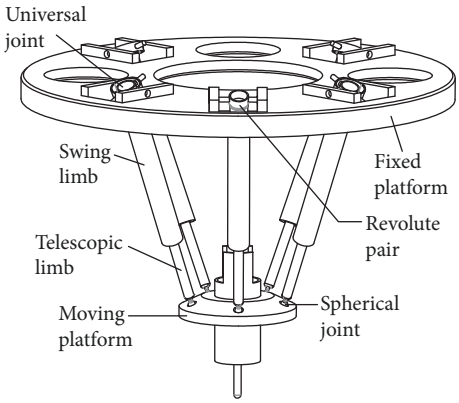

Figure 1: 4-UPS-RPS parallel mechanism.

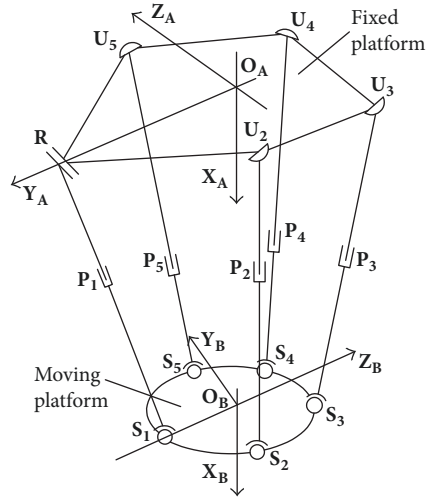

Figure 2: Coordinate system of 4-UPS-RPS parallel mechanism.

to the clearance value by using bifurcation diagrams. But up to now, the previous studies mainly concentrated on planar mechanism and focused on the nonlinearity caused by flexible member, clearance, dry friction, and bearing oil film, respectively, and rarely involved the bifurcation and chaotic behaviors analysis of spatial high-speed parallel mechanism with joint clearance and nonlinear deformation of the limbs.

The main purpose of this paper provides a methodology for forecasting the dynamics behavior of parallel mechanisms with clearance and flexible links and selecting appropriate system parameters of the mechanism. Under this background, this paper takes 4-UPS-RPS five-degree-of-freedom (namely, two moveable degrees and three rotational degrees) spatial parallel mechanism as the object (see in Figure 1)' a nonlinear dynamic model of the mechanism considering the joint clearance and flexible links is established by combining the KED method and Lagrange method, and the dynamics behaviors of the mechanism are analyzed.

2. Clearance Model and Contact Force Model of Spherical Joint

2.1. Spherical Clearance Model. The coordinate system of 4-UPS-RPS parallel mechanism is shown in Figure 2. As everyone knows, because of clearance, the degree of freedom (DOF) of the spherical joint has changed from 3 to 6. The configuration of spherical joint with clearance is shown in Figure 3. From Figure 3, there are three different types of relative motion between the ball and the socket, namely, continuous contact motion, free flight motion, and impact. The coordinate system of spherical joint with clearance is shown in Figure 4. From Figure 4, the centers of socket are defined as S_5, the centers of ball are defined as b_5, the unit tangent vector is defined as ${}^A\mathbf{t}$, the unit normal vector is defined as ${}^A\mathbf{n}$, and ${}^A\mathbf{P}_{S5}$ and ${}^A\mathbf{P}_{b5}$ are the position vectors of socket and ball in the fixed coordinate system, respectively.

$$\begin{aligned} {}^A\mathbf{P}_{S5} &= {}^A_B\mathbf{R}\,{}^B\mathbf{P}_{S5} + {}^A\mathbf{P}_{\mathrm{BO}}, \\ {}^A\mathbf{P}_{b5} &= {}^A_B\mathbf{R}^*\,{}^B\mathbf{P}_{S5} + {}^A\mathbf{P}_{\mathrm{BO}}{}^*, \end{aligned} \tag{1}$$

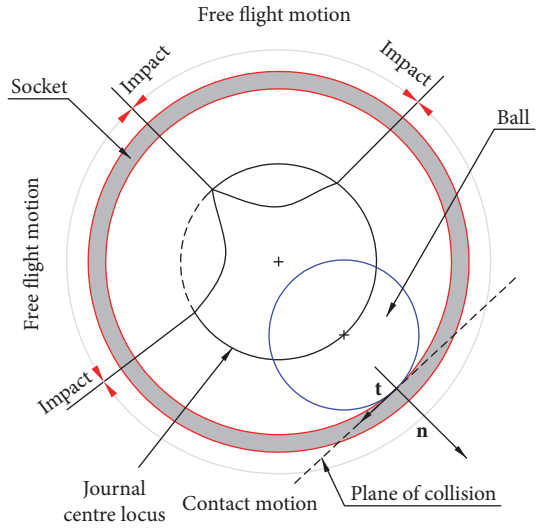

Figure 3: Configuration of spherical joint with clearance.

where ${}^A_B\mathbf{R}$ is the transfer matrix from moving coordinate system to fixed coordinate system. ${}^B\mathbf{P}_{S5}$ is the position vectors of socket in the moving coordinate system. ${}^A\mathbf{P}_{\mathrm{BO}}$ is the center coordinate of moving platform in the fixed coordinate system. ${}^A_B\mathbf{R}^*$ and ${}^A\mathbf{P}_{\mathrm{BO}}{}^*$ are the transfer matrix from moving coordinate system to fixed coordinate system and the center coordinate with clearance, respectively.

Then the vector of eccentricity is expressed as

$${}^A\mathbf{e} = {}^A\mathbf{P}_{b5} - {}^A\mathbf{P}_{S5}. \tag{2}$$

The relative penetration depth at t_n, t_{n+1} moments are defined as $\delta(t_n)$ and $\delta(t_{n+1})$, respectively. If $\delta(t_n)\delta(t_{n+1}) \le 0$, there is at least one collision between the two discrete time points [14].

The relative penetration depth defined as δ can be evaluated as

$$\delta = e - c, \tag{3}$$

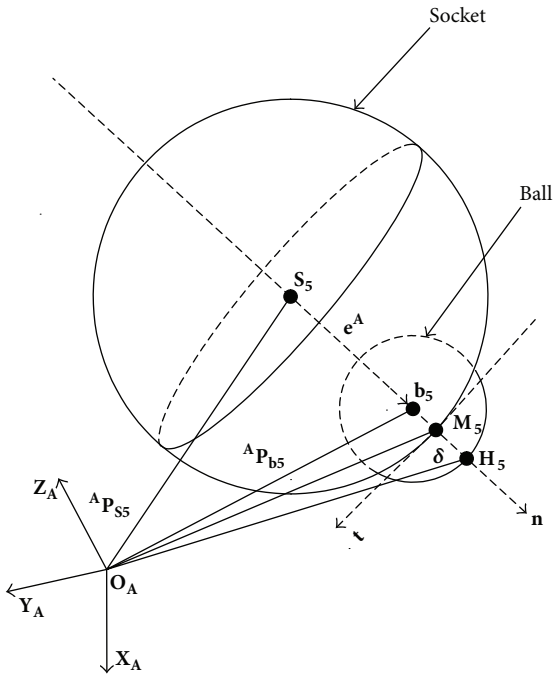

Figure 4: Coordinate system of spherical joint with clearance.

where e is the magnitude of the eccentricity vector, and $e = \sqrt{{}^A\mathbf{e}^T \cdot {}^A\mathbf{e}} = \sqrt{{}^Ae_x^2 + {}^Ae_y^2 + {}^Ae_z^2}$, c is joint clearance, and $c = R_{S5} - R_{b5}$, and R_{S5} and R_{b5} are the radius of socket and ball, respectively.

The unit vector normal to the collision surface between the socket and the ball is defined as $\mathbf{n}$, and $\mathbf{n}$ can be given by

$$\mathbf{n} = \frac{\mathbf{e}^A}{e}. \tag{4}$$

The fixed coordinate position of contact points defined as ${}^A\mathbf{P}_{M5}$ and ${}^A\mathbf{P}_{H5}$ are given by

$$\begin{aligned} {}^A\mathbf{P}_{M5} &= {}^A\mathbf{P}_{S5} + R_{s5}{}^A\mathbf{n}, \\ {}^A\mathbf{P}_{H5} &= {}^A\mathbf{P}_{b5} + R_{b5}{}^A\mathbf{n}. \end{aligned} \tag{5}$$

The velocity of the contact points defined as ${}^A\dot{\mathbf{P}}_{M5}$ and ${}^A\dot{\mathbf{P}}_{H5}$ are written as

$$\begin{aligned} {}^A\dot{\mathbf{P}}_{M5} &= {}^A\dot{\mathbf{P}}_{S5} + R_{S5}{}^A\dot{\mathbf{n}}, \\ {}^A\dot{\mathbf{P}}_{H5} &= {}^A\dot{\mathbf{P}}_{b5} + R_{b5}{}^A\dot{\mathbf{n}}, \end{aligned} \tag{6}$$

where $\dot{\mathbf{n}}$ is evaluated by differentiating $\mathbf{n}$.

Then the relative normal velocity and the relative tangential velocity defined as $\mathbf{V}_n$ and $\mathbf{V}_t$ can be expressed as

$$\begin{aligned} \mathbf{V}_n &= \left[\left({}^A\dot{\mathbf{P}}_{H5} - {}^A\dot{\mathbf{P}}_{M5}\right)^T {}^A\mathbf{n}\right] {}^A\mathbf{n}, \\ \mathbf{V}_t &= \left({}^A\dot{\mathbf{P}}_{H5} - {}^A\dot{\mathbf{P}}_{M5}\right) - {}^A\mathbf{V}_n. \end{aligned} \tag{7}$$

2.2. Normal and Tangential Contact Force Model. As we all know, the calculation of the normal contact force is the crucial factor in the dynamic study of mechanical systems with clearance. Apparently, the contact force model must take into account the impact velocity, the deformation, physical material properties of the colliding bodies, and geometry characteristics of the colliding bodies. Many scholars have done a lot of work on the improvement of the contact force model, such as Lankarani and Nikravesh [5], Flores et al. [15], Gonthier et al. [16], and Qin Zhiying and Lu Qishao [17]. Nowadays, the model proposed by Lankarani and Nikravesh (L-N model), which considers the damping hysteresis effect and accounts for the energy loss due to internal damping during the impact process, has been widely used. Therefore the L-N model is chosen in this paper. And the normal contact force can be expressed as

$$\mathbf{F}_n = K\boldsymbol{\delta}^n + D\dot{\boldsymbol{\delta}}, \tag{8}$$

where $\dot{\boldsymbol{\delta}}$ is the contact deformation velocity, the exponent $n = 3/2$, K is the stiffness coefficient, and

$$K = \frac{4}{3\left(\delta_{s5} + \delta_{b5}\right)} \sqrt{\frac{R_{s5}R_{b5}}{R_{s5} + R_{b5}}}, \tag{9}$$

where $\delta_{s5} = (1 - \nu_{s5})/E_{s5}$, $\delta_{b5} = (1 - \nu_{b5})/E_{b5}$, and ν_{s5} and ν_{b5} are Poisson ratios of socket and ball, respectively. E_{s5} and E_{b5} are Young's modulus of socket and ball, respectively. By definition, the radius is negative for concave surfaces and positive for convex surface.

D is the hysteresis damping coefficient used to describe the loss of energy during the collision, and

$$D = \frac{3K\delta^n\left(1 - {c_e}^2\right)}{4\dot{\delta}_0}, \tag{10}$$

where c_e, $\dot{\delta}_0$ are the restitution coefficient and the initial impact velocity, respectively.

The tangential contact characteristic of clearance is represented using Coulomb's friction law. However, there is a significant shortage of the classical Coulomb's friction law in describing the tangential friction of the clearance joint, when the value of the tangential velocity approaches zero. The modified Coulomb's friction model proposed by Ambrósio [18] can avoid numerical difficulties. The expression of tangential contact force can be expressed as

$$\mathbf{F}_t = -\mu_d c_d \mathbf{F}_n, \tag{11}$$

where μ_d is the friction coefficient. c_d is the dynamic correction coefficient, and

$$c_d = \begin{cases} 0, & |V|_t < V_0 \\ \dfrac{|V|_t - V_0}{V_1 - V_0}, & V_0 \le |V|_t \le V_1 \\ 1, & |V|_t > V_1, \end{cases} \tag{12}$$

where V_0 and V_1 are the given tolerances for the tangential velocity and $V_0 = 1.0 \times 10^{-4}$ m/s, $V_1 = 0.5$ m/s, respectively [19]. The dynamic correction coefficient can prevent that the frictional force changes direction when the tangential velocity is in the vicinity of zero.

Then the contact force of the clearance joint can be written as

$$\mathbf{F}_f = \mathbf{F}_n {}^A\mathbf{n} + \mathbf{F}_t {}^A\mathbf{t} = \begin{bmatrix} F_{fx} & F_{fy} & F_{fz} \end{bmatrix}^T. \tag{13}$$

3. Nonlinear Dynamic Model of 4-UPS-RPS Parallel Mechanism with Joint Clearance and Flexible Links

The 4-UPS-RPS (U represents universal joint; P represents prismatic joint; S represents spherical joint) parallel mechanism is composed of a fixed platform, a moving platform, and five driving limbs. The fixed platform is connected with the moving platform by four identical $U_iP_iS_i$ ($i = 2, 3, 4, 5$) limbs and another RP_1S_1 limb, as shown in Figure 1. The movement of the mechanism with joint clearance and flexible links is considered as the synthesis of two kinds of motion: one is the motion of the rigid mechanism with clearances and the other is elastic deformation motion caused by the mechanism with flexible links. Therefore, we should establish rigid body dynamic model of parallel mechanism with clearance and, on this basis, establish dynamic model of parallel mechanism with flexible links and joint clearance.

3.1. Rigid Body Dynamic Model of Parallel Mechanism with Joint Clearance. In 4-UPS-RPS spatial parallel mechanism, the spherical joint, which connects driving rods and the moving platform, is more representative. Therefore, the spherical joint clearance can reflect the influence of joint clearance on the dynamics behaviors of the mechanism [20]. In order to simplify the dynamics model, we consider that there is one spherical joint clearance in driving limb 5. The rigid body dynamic model of 4-UPS-RPS spatial parallel mechanism with clearance is established by Lagrange method.

3.1.1. Kinetic Energy of Mechanism with Clearance. The kinetic energy of the system consists of three parts: (i) the swing rod has only rotational kinetic energy around the center of the joint; (ii) the telescopic rod simultaneously has rotational kinetic energy and translational kinetic energy; (iii) the moving platform also has rotational kinetic energy and translational kinetic energy.

The length of the rod is defined as the distance between the center of the ball and the center of the universal joint. The length of driving limb 5 is unchanged when compared with the ideal case, the other four driving rods are influenced by the spherical clearance of driving limb 5, and some variables have changed, such as the length of a limb. We add symbols $*$ to indicate the amount of variables affected by the clearance.

The kinetic energy of moving platform, swing rod, and telescopic rod can be, respectively, written as

$$\begin{aligned}
\mathbf{E}_0^* &= \frac{1}{2}\left(m_0 \mathbf{v}_0^{*2} + \mathbf{J}_0 \boldsymbol{\omega}_0^{*2}\right), \\
\mathbf{E}_s^* &= \frac{1}{2}\left(\sum_{i=1}^{4} {}^A\boldsymbol{\omega}_i^{*T}\left({}^1\mathbf{J}_i^*\right){}^A\boldsymbol{\omega}_i^* + {}^A\boldsymbol{\omega}_5^T\left({}^1\mathbf{J}_5\right){}^A\boldsymbol{\omega}_5\right), \\
\mathbf{E}_t^* &= \frac{1}{2}\left(\sum_{i=1}^{4} {}^A\boldsymbol{\omega}_i^{*T}\left({}^2\mathbf{J}_i^*\right){}^A\boldsymbol{\omega}_i^* + {}^A\boldsymbol{\omega}_5^T\left({}^2\mathbf{J}_5\right){}^A\boldsymbol{\omega}_5\right. \\
&\quad \left. + \sum_{i=1}^{4} m_2 \dot{\mathbf{l}}_i^{*2} + m_2 \dot{\mathbf{l}}_5^2\right),
\end{aligned} \tag{14}$$

where m_0 is the mass of the moving platform. $\mathbf{J}_0$ is rotating inertia of moving platform. $\dot{\mathbf{l}}_5$ is the velocity of driving limb 5. $\mathbf{v}_0^*$ and $\boldsymbol{\omega}_0^*$ are the velocity and angular velocity of the moving platform with clearance, respectively. ${}^A\boldsymbol{\omega}_5$ is the angular velocity of the driving limb 5. ${}^1\mathbf{J}_5$ and ${}^2\mathbf{J}_5$ represent the inertia matrix of swing rod and telescopic rod of driving limb 5. $\dot{\mathbf{l}}_i^*$ is the velocity of driving limb i ($i = 1, 2, 3, 4$) with clearance.

${}^k\mathbf{J}_i^*$ ($k = 1, 2$, $i = 1, 2, 3, 4$) is the inertia matrix of driving limb with clearance. m_k is the mass of driving rod. $k = 1$ represents the swing rod and $k = 2$ represents telescopic rod.

$${}^k\mathbf{J}_i^* = \mathbf{R}'^* \begin{bmatrix} \mathbf{I}_{xx} + m_k\mathbf{r}_k^2 & 0 & 0 \\ 0 & \mathbf{I}_{yy} + m_k\mathbf{r}_k^2 & 0 \\ 0 & 0 & \mathbf{I}_{zz} \end{bmatrix} \mathbf{R}'^{*T}, \tag{15}$$

where $\mathbf{R}'^*$ is transfer matrix. m_k is the mass of driving rod. $\mathbf{r}_k$ is the distance between the center of driving rod and the corresponding joint of the fixed platform.

${}^A\boldsymbol{\omega}_i^*$ ($i = 1, 2, 3, 4$) represents angular velocity of driving limb i with clearance.

$$\begin{aligned}
{}^A\boldsymbol{\omega}_i^* = \frac{1}{|\mathbf{l}_i^*|}\Bigg(& {}^A\widehat{\mathbf{n}}_i^* \\
& - {}^A\widehat{\mathbf{n}}_i^* {}^A\widehat{\mathbf{r}}_{\mathbf{si}}^* \begin{bmatrix} 0 & -\sin\boldsymbol{\alpha}^* & \cos\boldsymbol{\alpha}^*\cos\boldsymbol{\beta}^* \\ 0 & \cos\boldsymbol{\alpha}^* & \sin\boldsymbol{\alpha}^*\cos\boldsymbol{\beta}^* \\ 1 & 0 & -\sin\boldsymbol{\beta}^* \end{bmatrix}\Bigg)\dot{\mathbf{q}}_c,
\end{aligned} \tag{16}$$

where ${}^A\widehat{\mathbf{n}}_i^* = \begin{bmatrix} 0 & -{}^A\mathbf{n}_{iz}^* & {}^A\mathbf{n}_{iy}^* \\ {}^A\mathbf{n}_{iz}^* & 0 & -{}^A\mathbf{n}_{ix}^* \\ -{}^A\mathbf{n}_{iy}^* & {}^A\mathbf{n}_{ix}^* & 0 \end{bmatrix}$, ${}^A\widehat{\mathbf{r}}_i^* = \begin{bmatrix} 0 & -{}^A\mathbf{r}_{iz}^* & {}^A\mathbf{r}_{iy}^* \\ {}^A\mathbf{r}_{iz}^* & 0 & -{}^A\mathbf{r}_{ix}^* \\ -{}^A\mathbf{r}_{iy}^* & {}^A\mathbf{r}_{ix}^* & 0 \end{bmatrix}$. ${}^A\mathbf{n}_i^*$ is the unit direction vector of driving limb i ($i = 1, 2, 3, 4$) in the fixed coordinate system with clearance; ${}^A\mathbf{n}_{ix}^*$, ${}^A\mathbf{n}_{iy}^*$, and ${}^A\mathbf{n}_{iz}^*$ are the components of ${}^A\mathbf{n}_i^*$ along the x-, y-, and z-axis, respectively. ${}^A\mathbf{r}_i^*$

is the position vector of spherical joint of driving limb i ($i = 1, 2, 3, 4$) relative to the center of the moving platform in the fixed coordinate system with clearance. ${}^{A}\mathbf{r}_{ix}^{*}$, ${}^{A}\mathbf{r}_{iy}^{*}$, and ${}^{A}\mathbf{r}_{iz}^{*}$ are the components of ${}^{A}\mathbf{r}_{i}^{*}$ along the x-, y-, and z-axis, respectively. $|\mathbf{l}_i^*|$ is the length of driving limb i ($i = 1, 2, 3, 4$) with clearance. $\boldsymbol{\alpha}^*$, $\boldsymbol{\beta}^*$, $\boldsymbol{\gamma}^*$ are the Euler angles describing the rotation of the moving platform with clearance. $\dot{\mathbf{q}}_c$ is the first-order derivative of rigid body position vectors of the center of moving platform with clearance $\mathbf{q}_c$, and $\mathbf{q}_c = \begin{bmatrix}\mathbf{q}_{cx} & \mathbf{q}_{cy} & \mathbf{q}_{cz} & \boldsymbol{\alpha}^* & \boldsymbol{\beta}^* & \boldsymbol{\gamma}^*\end{bmatrix}^T$.

Then the kinetic energy of the mechanism with clearance can be expressed as

$$\mathbf{E}^* = \mathbf{E}_0^* + \mathbf{E}_\mathbf{s}^* + \mathbf{E}_\mathbf{t}^*. \tag{17}$$

3.1.2. Potential Energy of Mechanism with Clearance. The OYZ plane in the fixed coordinate system is chosen as the zero potential energy surface. The system potential energy consists of three parts, and the potential energy of moving platform, swing rod, and telescopic rod are, respectively, given by

$$\mathbf{W}_0^* = -m_0 g {}^{\mathbf{A}}\mathbf{x}_0^* \tag{18}$$

$$\mathbf{W}_\mathbf{s}^* = -\sum_{i=1}^{4} m_1 g \mathbf{S}_{ix}^* \frac{|\mathbf{l}_{sc}|}{|\mathbf{l}_i^*|} - m_1 g \mathbf{S}_{5x} \frac{|\mathbf{l}_{sc}|}{|\mathbf{l}_5|}, \tag{19}$$

$$\begin{aligned}\mathbf{W}_\mathbf{t}^* = &-\sum_{i=1}^{4} m_2 g \mathbf{S}_{ix}^* \left(1 - \frac{|\mathbf{l}_{tc}^*|}{|\mathbf{l}_i^*|}\right) \\ &- m_2 g \mathbf{S}_{5x} \left(1 - \frac{|\mathbf{l}_{tc}|}{|\mathbf{l}_5|}\right),\end{aligned} \tag{20}$$

where $\mathbf{x}_0^*$ is the X component of the center coordinate of moving platform in fixed coordinate system; $\mathbf{S}_{5x}$ is the X component of spherical joint center coordinate in fixed coordinate system. $|\mathbf{l}_{sc}|$ is the distance between the center of swing rod and the center of universal joint. $|\mathbf{l}_{tc}|$ is the distance between the center of telescopic rod and the center of spherical joint. $|\mathbf{l}_5|$ is the length of the driving limb 5. $\mathbf{S}_{ix}^*$ and $|\mathbf{l}_{tc}^*|$ are the variables of driving limb i ($i = 1, 2, 3, 4$) with clearance, respectively.

The potential energy of the mechanism with clearance can be expressed as

$$\mathbf{W}^* = \mathbf{W}_0^* + \mathbf{W}_\mathbf{s}^* + \mathbf{W}_\mathbf{t}^*. \tag{21}$$

3.1.3. Dynamic Model of Parallel Mechanism with Clearance. The driving forces of 4-UPS-RPS spatial parallel mechanism are defined as $\mathbf{f} = \begin{bmatrix}\mathbf{f}_1 & \mathbf{f}_2 & \mathbf{f}_3 & \mathbf{f}_4 & \mathbf{f}_5\end{bmatrix}^T$. Then the generalized forces corresponding to the driving forces can be expressed as

$$\mathbf{Q}_d = \mathbf{G}^* \mathbf{f} = \mathbf{J}_A^{*T} \mathbf{f}, \tag{22}$$

where $\mathbf{J}_A^*$ is velocity Jacobian matrix. $\mathbf{G}^*$ is the transpose of $\mathbf{J}_A^*$, namely, the dual relation between velocity mapping and force mapping.

The contact force transformed into fixed coordinate system can be written as

$$\begin{bmatrix}\mathbf{F}_f & \mathbf{M}_f\end{bmatrix}^T = \begin{bmatrix}{}^{\mathbf{A}}\mathbf{F}_{fx} & {}^{\mathbf{A}}\mathbf{F}_{fx} & {}^{\mathbf{A}}\mathbf{F}_{fx} & 0 & 0 & 0\end{bmatrix}^T. \tag{23}$$

And the generalized force corresponding to the contact force can be expressed as

$$\mathbf{Q}_c = \mathbf{J}_{2A}^T \begin{bmatrix}\mathbf{F}_f & \mathbf{M}_f\end{bmatrix}^T, \tag{24}$$

where $\mathbf{J}_{2A}$ is the velocity transfer matrix from generalized coordinate system to Cartesian coordinate system, and $\mathbf{J}_{2A}^T = \begin{bmatrix} 1 & & & & & \\ & 1 & & & & \\ & & 1 & & & \\ & & & -\sin\boldsymbol{\alpha}^* & \cos\boldsymbol{\alpha}^* \cos\boldsymbol{\beta}^* & \\ & & & \cos\boldsymbol{\alpha}^* & \sin\boldsymbol{\alpha}^* \cos\boldsymbol{\beta}^* & \\ & & 1 & & -\sin\boldsymbol{\beta}^* & \end{bmatrix}^T$.

The equivalent generalized force corresponding to the nonconservative force of the system can be expressed as

$$\mathbf{Q}_k = \mathbf{Q}_d + \mathbf{Q}_c. \tag{25}$$

Taking (17), (21), and (25) into the Lagrange equation, the rigid body dynamic model of parallel mechanism with joint clearance is expressed as

$$\begin{aligned}
\ddot{\mathbf{q}}_{cx} &= f_1\left(\mathbf{t}, \mathbf{q}_{cx}, \mathbf{q}_{cy}, \mathbf{q}_{cz}, \boldsymbol{\alpha}^*, \boldsymbol{\beta}^*, \boldsymbol{\gamma}^*, \dot{\mathbf{q}}_{cx}, \dot{\mathbf{q}}_{cy}, \dot{\mathbf{q}}_{cz}, \dot{\boldsymbol{\alpha}}^*, \dot{\boldsymbol{\beta}}^*, \dot{\boldsymbol{\gamma}}^*\right), \\
\ddot{\mathbf{q}}_{cy} &= f_2\left(\mathbf{t}, \mathbf{q}_{cx}, \mathbf{q}_{cy}, \mathbf{q}_{cz}, \boldsymbol{\alpha}^*, \boldsymbol{\beta}^*, \boldsymbol{\gamma}^*, \dot{\mathbf{q}}_{cx}, \dot{\mathbf{q}}_{cy}, \dot{\mathbf{q}}_{cz}, \dot{\boldsymbol{\alpha}}^*, \dot{\boldsymbol{\beta}}^*, \dot{\boldsymbol{\gamma}}^*\right), \\
\ddot{\mathbf{q}}_{cz} &= f_3\left(\mathbf{t}, \mathbf{q}_{cx}, \mathbf{q}_{cy}, \mathbf{q}_{cz}, \boldsymbol{\alpha}^*, \boldsymbol{\beta}^*, \boldsymbol{\gamma}^*, \dot{\mathbf{q}}_{cx}, \dot{\mathbf{q}}_{cy}, \dot{\mathbf{q}}_{cz}, \dot{\boldsymbol{\alpha}}^*, \dot{\boldsymbol{\beta}}^*, \dot{\boldsymbol{\gamma}}^*\right), \\
\ddot{\boldsymbol{\alpha}}^* &= f_4\left(\mathbf{t}, \mathbf{q}_{cx}, \mathbf{q}_{cy}, \mathbf{q}_{cz}, \boldsymbol{\alpha}^*, \boldsymbol{\beta}^*, \boldsymbol{\gamma}^*, \dot{\mathbf{q}}_{cx}, \dot{\mathbf{q}}_{cy}, \dot{\mathbf{q}}_{cz}, \dot{\boldsymbol{\alpha}}^*, \dot{\boldsymbol{\beta}}^*, \dot{\boldsymbol{\gamma}}^*\right), \\
\ddot{\boldsymbol{\beta}}^* &= f_5\left(\mathbf{t}, \mathbf{q}_{cx}, \mathbf{q}_{cy}, \mathbf{q}_{cz}, \boldsymbol{\alpha}^*, \boldsymbol{\beta}^*, \boldsymbol{\gamma}^*, \dot{\mathbf{q}}_{cx}, \dot{\mathbf{q}}_{cy}, \dot{\mathbf{q}}_{cz}, \dot{\boldsymbol{\alpha}}^*, \dot{\boldsymbol{\beta}}^*, \dot{\boldsymbol{\gamma}}^*\right), \\
\ddot{\boldsymbol{\gamma}}^* &= f_6\left(\mathbf{t}, \mathbf{q}_{cx}, \mathbf{q}_{cy}, \mathbf{q}_{cz}, \boldsymbol{\alpha}^*, \boldsymbol{\beta}^*, \boldsymbol{\gamma}^*, \dot{\mathbf{q}}_{cx}, \dot{\mathbf{q}}_{cy}, \dot{\mathbf{q}}_{cz}, \dot{\boldsymbol{\alpha}}^*, \dot{\boldsymbol{\beta}}^*, \dot{\boldsymbol{\gamma}}^*\right).
\end{aligned} \tag{26}$$

3.2. Dynamic Model of Parallel Mechanism with Joint Clearance and Flexible Links

3.2.1. Model of the Beam Element. The swing rod, moving platform, and fixed platform of 4-UPS-RPS parallel mechanism are regarded as rigid; the telescopic rod P_iS_i ($i = 1, 2, 3, 4, 5$) is regarded as flexible. The space rectangular beam

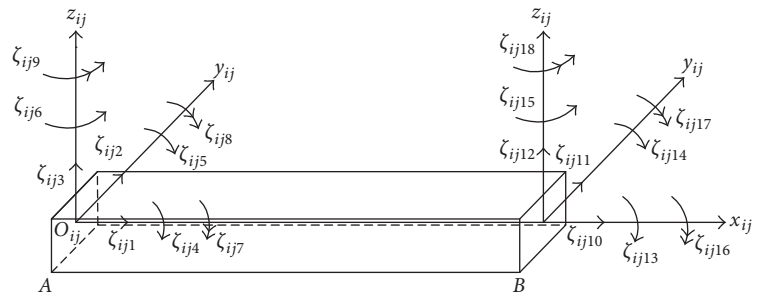

Figure 5: Space rectangular beam element.

element is adopted to model the 4-UPS-RPS spatial parallel mechanism, as shown in Figure 5. $\boldsymbol{\zeta}_{ij1} \cdots \boldsymbol{\zeta}_{ij3}$ and $\boldsymbol{\zeta}_{ij10} \cdots \boldsymbol{\zeta}_{ij12}$, $\boldsymbol{\zeta}_{ij4} \cdots \boldsymbol{\zeta}_{ij6}$ and $\boldsymbol{\zeta}_{ij13} \cdots \boldsymbol{\zeta}_{ij15}$, $\boldsymbol{\zeta}_{ij7} \cdots \boldsymbol{\zeta}_{ij9}$ and $\boldsymbol{\zeta}_{ij16} \cdots \boldsymbol{\zeta}_{ij18}$ are elastic displacements, elastic angular displacements, and curvatures of nodes A and B, respectively.

3.2.2. Dynamic Equation of the Beam Element. The elastic displacements of arbitrary point $(\mathbf{x}_{ij})$ defined as $\mathbf{u}(\mathbf{x}_{ij}, \mathbf{t})$, $\mathbf{v}(\mathbf{x}_{ij}, \mathbf{t})$, $\mathbf{w}(\mathbf{x}_{ij}, \mathbf{t})$ and the elastic angle displacements of arbitrary point $(\mathbf{x}_{ij})$ defined as $\psi_x(\mathbf{x}_{ij}, \mathbf{t})$, $\psi_y(\mathbf{x}_{ij}, \mathbf{t})$, $\psi_z(\mathbf{x}_{ij}, \mathbf{t})$ can be, respectively, expressed as

$$\begin{aligned}
\mathbf{u}\left(\mathbf{x}_{ij}, \mathbf{t}\right) &= \mathbf{P}_{ij1}^T \boldsymbol{\zeta}_{ij} \\
\mathbf{v}\left(\mathbf{x}_{ij}, \mathbf{t}\right) &= \mathbf{P}_{ij2}^T \boldsymbol{\zeta}_{ij} \\
\mathbf{w}\left(\mathbf{x}_{ij}, \mathbf{t}\right) &= \mathbf{P}_{ij3}^T \boldsymbol{\zeta}_{ij} \\
\psi_x\left(\mathbf{x}_{ij}, \mathbf{t}\right) &= \mathbf{P}_{ij4}^T \boldsymbol{\zeta}_{ij} \\
\psi_y\left(\mathbf{x}_{ij}, \mathbf{t}\right) &= \left(\frac{\partial \mathbf{P}_{ij3}}{\partial \mathbf{x}_{ij}}\right)^T \boldsymbol{\zeta}_{ij} \\
\psi_z\left(\mathbf{x}_{ij}, \mathbf{t}\right) &= \left(\frac{\partial \mathbf{P}_{ij2}}{\partial \mathbf{x}_{ij}}\right)^T \boldsymbol{\zeta}_{ij},
\end{aligned} \tag{27}$$

where $\boldsymbol{\zeta}_{ij} = \left[\zeta_{ij1} \;\; \zeta_{ij2} \;\; \cdots \;\; \zeta_{ij18}\right]^T$, $\mathbf{P}_{ij1} \cdots \mathbf{P}_{ij4}$ are interpolated vectors and can be written as

$$\begin{aligned}
&\mathbf{P}_{ij1} \\
&= \left[1 - \sigma \;\; 0 \;\; 0 \;\; 0 \;\; 0 \;\; 0 \;\; 0 \;\; 0 \;\; 0 \;\; \sigma \;\; 0 \;\; 0 \;\; 0 \;\; 0 \;\; 0 \;\; 0 \;\; 0 \;\; 0\right], \\
&\mathbf{P}_{ij2} \\
&= \left[0 \;\; \boldsymbol{\xi}_1 \;\; 0 \;\; 0 \;\; 0 \;\; \boldsymbol{\xi}_2 \;\; 0 \;\; 0 \;\; \boldsymbol{\xi}_3 \;\; 0 \;\; \boldsymbol{\xi}_4 \;\; 0 \;\; 0 \;\; 0 \;\; \boldsymbol{\xi}_5 \;\; 0 \;\; 0 \;\; \boldsymbol{\xi}_6\right], \\
&\mathbf{P}_{ij3} \\
&= \left[0 \;\; 0 \;\; \boldsymbol{\xi}_1 \;\; 0 \;\; \boldsymbol{\xi}_2 \;\; 0 \;\; 0 \;\; \boldsymbol{\xi}_3 \;\; 0 \;\; 0 \;\; 0 \;\; \boldsymbol{\xi}_4 \;\; 0 \;\; \boldsymbol{\xi}_5 \;\; 0 \;\; 0 \;\; \boldsymbol{\xi}_6 \;\; 0\right], \\
&\mathbf{P}_{ij4} \\
&= \left[0 \;\; 0 \;\; 0 \;\; \boldsymbol{\xi}_7 \;\; 0 \;\; 0 \;\; \boldsymbol{\xi}_8 \;\; 0 \;\; 0 \;\; 0 \;\; 0 \;\; 0 \;\; \boldsymbol{\xi}_9 \;\; 0 \;\; 0 \;\; \boldsymbol{\xi}_{10} \;\; 0 \;\; 0\right],
\end{aligned}$$

$$\begin{aligned}
\boldsymbol{\xi}_1 &= 1 - 10\sigma^3 + 15\sigma^4 - 6\sigma^5, \\
\boldsymbol{\xi}_2 &= \mathbf{lu}_{ij}\left(\sigma - 6\sigma^3 + 8\sigma^4 - 3\sigma^5\right), \\
\boldsymbol{\xi}_3 &= \frac{1}{2}\mathbf{lu}_{ij}^2\left(\sigma^2 - 3\sigma^3 + 3\sigma^4 - \sigma^5\right), \\
\boldsymbol{\xi}_4 &= 10\sigma^3 - 15\sigma^4 + 6\sigma^5, \\
\boldsymbol{\xi}_5 &= \mathbf{lu}_{ij}\left(-4\sigma^3 + 7\sigma^4 - 3\sigma^5\right), \\
\boldsymbol{\xi}_6 &= \frac{1}{2}\mathbf{lu}_{ij}^2\left(\sigma^3 - 2\sigma^4 + \sigma^5\right), \\
\boldsymbol{\xi}_7 &= 1 - 3\sigma^2 + 2\sigma^3, \\
\boldsymbol{\xi}_8 &= \mathbf{lu}_{ij}\left(\sigma - 2\sigma^2 + \sigma^3\right), \\
\boldsymbol{\xi}_9 &= 3\sigma^2 - 2\sigma^3, \\
\boldsymbol{\xi}_{10} &= \mathbf{lu}_{ij}\left(-\sigma^2 + \sigma^3\right).
\end{aligned} \tag{28}$$

And $\sigma = \mathbf{x}_{ij}/\mathbf{lu}_{ij}$, $\mathbf{lu}_{ij}$ is the length of unit j.

The kinetic energy of the unit consists of two parts: the translational kinetic energy and the rotational kinetic energy. The kinetic energy of the unit can be written as

$$\begin{aligned}
\mathbf{T} = \frac{1}{2}\int_0^{\mathbf{lu}_{ij}} m(x)\left[\left(\frac{\mathbf{du_a}\left(\mathbf{x}_{ij}, \mathbf{t}\right)}{\mathbf{dt}}\right)^2 + \left(\frac{\mathbf{dv_a}\left(\mathbf{x}_{ij}, \mathbf{t}\right)}{\mathbf{dt}}\right)^2\right. \\
\left. + \left(\frac{\mathbf{dw_a}\left(\mathbf{x}_{ij}, \mathbf{t}\right)}{\mathbf{dt}}\right)^2\right]\mathbf{dx} + \frac{1}{2} \\
\cdot \int_0^{\mathbf{lu}_{ij}} \rho \mathbf{I}_p \left(\frac{\mathbf{d}\psi_{\mathbf{xa}}\left(\mathbf{x}_{ij}, \mathbf{t}\right)}{\mathbf{dt}}\right)^2 \mathbf{dx},
\end{aligned} \tag{29}$$

where ρ is the mass density of the beam element. $\mathbf{I}_p$ is the polar moment of inertia of unit cross-sectional area to the x-axis, $m(x)$ is the mass of beam element. $\mathbf{u_a}(\mathbf{x}_{ij}, \mathbf{t})$, $\mathbf{v_a}(\mathbf{x}_{ij}, \mathbf{t})$, $\mathbf{w_a}(\mathbf{x}_{ij}, \mathbf{t})$, $\psi_{\mathbf{xa}}(\mathbf{x}_{ij}, \mathbf{t})$ are the absolute displacements and the absolute angle displacements, respectively.

Equation (29) can be simply written as

$$\mathbf{T} = \frac{1}{2}\left(\dot{\boldsymbol{\zeta}}_{ij} + \dot{\boldsymbol{\zeta}}_{ijr}\right)^T \mathbf{M}_e \left(\dot{\boldsymbol{\zeta}}_{ij} + \dot{\boldsymbol{\zeta}}_{ijr}\right), \tag{30}$$

where $\mathbf{M}_e = \int_0^{\mathbf{lu}_{ij}} [\rho A(\mathbf{P}_{ij1}^T \mathbf{P}_{ij1} + \mathbf{P}_{ij2}^T \mathbf{P}_{ij2} + \mathbf{P}_{ij3}^T \mathbf{P}_{ij3}) + \rho \mathbf{I}_p (\mathbf{P}_{ij4}^T \mathbf{P}_{ij4})] \mathbf{dx}$, $\dot{\boldsymbol{\zeta}}_{ij}$ and $\dot{\boldsymbol{\zeta}}_{ijr}$ are the elastic velocities of the unit nodes and the rigid body velocities of the unit nodes, and A is the cross-sectional area of element.

The deformation energy of the unit consists of three parts: bending deformation energy, tension/compression deformation energy, and torsional deformation energy. The deformation energy of the unit can be written as

$$\mathbf{V} = \frac{1}{2} E \int_0^{\mathbf{lu}_{ij}} \left[A \left(\frac{\partial \mathbf{u}\left(\mathbf{x}_{ij}, \mathbf{t}\right)}{\partial \mathbf{x}} \right)^2 + \mathbf{I}_z \left(\frac{\partial^2 \mathbf{v}\left(\mathbf{x}_{ij}, \mathbf{t}\right)}{\partial \mathbf{x}^2} \right)^2 + \mathbf{I}_y \left(\frac{\partial^2 \mathbf{w}\left(\mathbf{x}_{ij}, \mathbf{t}\right)}{\partial \mathbf{x}^2} \right)^2 \right] \mathbf{dx} + \frac{1}{2} \cdot \int_0^{\mathbf{lu}_{ij}} G \mathbf{I}_p \left(\frac{\partial \psi_{\mathbf{x}}\left(\mathbf{x}_{ij}, \mathbf{t}\right)}{\partial \mathbf{x}} \right)^2 \mathbf{dx}, \tag{31}$$

where E is Young's modulus of the beam element; G is the shear elastic modulus of the beam element. $\mathbf{I}_y$ is principal moment of inertia of unit cross section to the y-axis; $\mathbf{I}_z$ is principal moment of inertia of unit cross section to the z-axis.

Equation (31) can be simply written as

$$\mathbf{V} = \frac{1}{2} \zeta_{ij}^T \mathbf{K}_e \zeta_{ij}, \tag{32}$$

where $\mathbf{K}_e = E[A \int_0^{\mathbf{lu}_{ij}} \mathbf{p}_{ij1}^T \mathbf{p}_{ij1} \mathbf{dx} + \mathbf{I}_z \int_0^{\mathbf{lu}_{ij}} \ddot{\mathbf{p}}_{ij2}^T \ddot{\mathbf{p}}_{ij2} \mathbf{dx} + \mathbf{I}_z \int_0^{\mathbf{lu}_{ij}} \ddot{\mathbf{p}}_{ij1}^T \ddot{\mathbf{p}}_{ij1} \mathbf{dx}] + G\mathbf{I}_p \int_0^{\mathbf{lu}_{ij}} \dot{\mathbf{p}}_{ij4}^T \dot{\mathbf{p}}_{ij4} \mathbf{dx}$.

When considering joint clearance, there is no kinematic constraint between the elements of the joint, and the interaction between elements is achieved by contact force treated as an external force. The telescopic rod is divided into space beam element; then the elastic dynamic equation of the beam element ij (that is j unit on the i telescopic rod) can be written as follows [21]:

$$\mathbf{M}_{ij} \ddot{\boldsymbol{\zeta}}_{ij} + \mathbf{C}_{ij} \dot{\boldsymbol{\zeta}}_{ij} + \mathbf{K}_{ij} \boldsymbol{\zeta} = \mathbf{Q}_{ij}^*, \tag{33}$$

where $\mathbf{M}_{ij}$, $\mathbf{C}_{ij}$, $\mathbf{K}_{ij}$ are mass matrix of element, damping matrix of element, and stiffness matrix of element; $\mathbf{Q}_{ij}^*$ is the generalized force matrix of unit, which contains element external force, such as contact force $\mathbf{F}_f$, force between units, rigid body inertial force array for system unit, and the elastic force $\mathbf{Qe}_{ij} = [\mathbf{Fe}\ \mathbf{Me}]^T$. The inertia force (**Fe**) and the moment of inertia (**Me**) of moving platform caused by the elastic deformation of driving limbs can be obtained by solving the elastodynamic equation. $\dot{\boldsymbol{\zeta}}_{ij}$, $\ddot{\boldsymbol{\zeta}}_{ij}$ are the first-order and second-order derivative of unit's generalized coordinate vector $\boldsymbol{\zeta}_{ij}$, respectively.

3.2.3. Dynamic Equation of Driving Limbs. Dividing telescopic rod $\mathbf{P}_i\mathbf{S}_i$ into m units is shown in Figure 6; the constraint conditions are as follows.

(1) The elastic displacement, elastic rotation angle, and curvature of the unit wrapped in rigid body are zero.

(2) The bottom point $\mathbf{B}_j$ of the j unit on the telescopic rod is coincident with the top point $\mathbf{A}_{j+1}$ of the $(j+1)$ unit.

(3) On the telescopic rod, the connecting part of the unit m and the moving platform is a spherical joint, and the three-curvature coordinate is zero.

According to the constraints of the motion units, the generalized coordinates can be written as

$$\mathbf{O}_i = [\boldsymbol{\zeta}_{i(n+1)1}\ \boldsymbol{\zeta}_{i(n+1)2}\ \cdots\ \boldsymbol{\zeta}_{i(n+1)9}\ \boldsymbol{\zeta}_{i(n+2)1}\ \cdots\ \boldsymbol{\zeta}_{i(n+2)9}\ \cdots\ \boldsymbol{\zeta}_{im1}\ \cdots\ \boldsymbol{\zeta}_{im9}\ \boldsymbol{\zeta}_{im10}\ \cdots\ \boldsymbol{\zeta}_{im15}]. \tag{34}$$

The relationship between $\mathbf{O}_i$ and generalized coordinates matrix of element $\boldsymbol{\zeta}_{ij}$ in fixed coordinate system is expressed as

$$\boldsymbol{\zeta}_{ij} = \overline{\mathbf{A}}_{ij} \mathbf{O}_i. \tag{35}$$

Then the elastic dynamic equation of driving limb i ($i = 1, 2, 3, 4, 5$) can be expressed as

$$\mathbf{M}^i \ddot{\mathbf{O}}_i + \mathbf{C}^i \dot{\mathbf{O}}_i + \mathbf{K}^i \mathbf{O}_i = \mathbf{Q}^{i*}, \tag{36}$$

where $\mathbf{M}^i$ is the mass matrix, and $\mathbf{M}^i = \sum_{j=1}^m \mathbf{M}_{ij}$. $\mathbf{C}^i$ is damping matrix, and $\mathbf{C}^i = \sum_{j=1}^m \mathbf{C}_{ij}$. $\mathbf{K}^i$ is stiffness matrix of rods, and $\mathbf{K}^i = \sum_{j=1}^m \mathbf{K}_{ij}$. $\mathbf{Q}^{i*}$ is the generalized force matrix of limb, and $\mathbf{Q}^{i*} = \sum_{j=1}^m \mathbf{Q}_{ij}^*$.

3.2.4. Elastic Dynamic Model of the Parallel Mechanism with Joint Clearance and Flexible Links. The kinematic constrain equations of the moving platform and the driving limbs can be expressed as

$$\mathbf{O}_{si} = \mathbf{J}_{si} \mathbf{O}_0, \tag{37}$$

where $\mathbf{O}_{si}$ is the elastic displacement of spherical joint $\mathbf{S}_i$ ($i = 1, 2, 3, 4, 5$), and $\mathbf{O}_{si} = [\Delta \mathbf{x}_{si}\ \Delta \mathbf{y}_{si}\ \Delta \mathbf{z}_{si}]^T$. $\mathbf{O}_0$ is the displacement of moving platform caused by elastic deformation of driving limbs, and $\mathbf{O}_0 = [\Delta \mathbf{X}_{\mathrm{BO}}\ \Delta \mathbf{Y}_{\mathrm{BO}}\ \Delta \mathbf{Z}_{\mathrm{BO}}\ \Delta \boldsymbol{\gamma}\ \Delta \boldsymbol{\beta}\ \Delta \boldsymbol{\alpha}]^T = [\mathbf{q}_1\ \mathbf{q}_2\ \mathbf{q}_3\ \mathbf{q}_4\ \mathbf{q}_5\ \mathbf{q}_6]^T$. $\mathbf{J}_{si}$ is kinematic constraint matrix, and

$$\mathbf{J}_{si} = \begin{bmatrix} 1 & 0 & 0 & 0 & {}^A\mathbf{Z}_{si} & -{}^A\mathbf{Y}_{si} \\ 0 & 1 & 0 & -{}^A\mathbf{Z}_{si} & 0 & {}^A\mathbf{X}_{si} \\ 0 & 0 & 1 & {}^A\mathbf{Y}_{si} & -{}^A\mathbf{X}_{si} & 0 \end{bmatrix}, \tag{38}$$

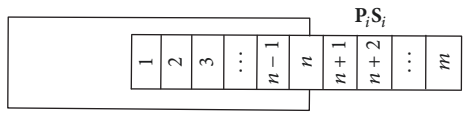

Figure 6: Unit of telescopic limb $\mathbf{P}_i\mathbf{S}_i$.

where ${}^A\mathbf{X}_{si}$, ${}^A\mathbf{Y}_{si}$, ${}^A\mathbf{Z}_{si}$ are the coordinates of spherical joint $\mathbf{S}_i$ in the fixed coordinate system.

According to the Newton-Euler equation, the dynamical constraint equations of the mechanism are written as

$$\begin{bmatrix} m_0 & & & & & & \\ & m_0 & & & & & \\ & & m_0 & & & & \\ & & & \mathbf{I}_{xx} & \mathbf{I}_{xy} & \mathbf{I}_{xz} & \\ & & & \mathbf{I}_{yx} & \mathbf{I}_{yy} & \mathbf{I}_{yz} & \\ & & & \mathbf{I}_{zx} & \mathbf{I}_{zy} & \mathbf{I}_{zz} & \end{bmatrix} \begin{bmatrix} \ddot{\mathbf{q}}_1 \\ \ddot{\mathbf{q}}_2 \\ \ddot{\mathbf{q}}_3 \\ \ddot{\mathbf{q}}_4 \\ \ddot{\mathbf{q}}_5 \\ \ddot{\mathbf{q}}_6 \end{bmatrix} = \begin{bmatrix} \sum \mathbf{F}_{ix} \\ \sum \mathbf{F}_{ix} \\ \sum \mathbf{F}_{iz} \\ \sum \mathbf{M}_{ix} \\ \sum \mathbf{M}_{ix} \\ \sum \mathbf{M}_{ix} \end{bmatrix} + \begin{bmatrix} \sum \mathbf{F}_{ox} \\ \sum \mathbf{F}_{oy} \\ \sum \mathbf{F}_{oz} \\ \sum \mathbf{M}_{ox} \\ \sum \mathbf{M}_{oy} \\ \sum \mathbf{M}_{oz} \end{bmatrix} - \begin{bmatrix} m_0 & & & & & & \\ & m_0 & & & & & \\ & & m_0 & & & & \\ & & & \mathbf{I}_{xx} & \mathbf{I}_{xy} & \mathbf{I}_{xz} & \\ & & & \mathbf{I}_{yx} & \mathbf{I}_{yy} & \mathbf{I}_{yz} & \\ & & & \mathbf{I}_{zx} & \mathbf{I}_{zy} & \mathbf{I}_{zz} & \end{bmatrix} \begin{bmatrix} \ddot{\mathbf{q}}_{cx} \\ \ddot{\mathbf{q}}_{cy} \\ \ddot{\mathbf{q}}_{cz} \\ \ddot{\boldsymbol{\gamma}}^* \\ \ddot{\boldsymbol{\beta}}^* \\ \ddot{\boldsymbol{\alpha}}^* \end{bmatrix}. \tag{39}$$

Equation (39) can be simply written as

$$\mathbf{M}_0\ddot{\mathbf{O}}_0 = \mathbf{f} + \mathbf{F}_0 - \mathbf{M}_0\ddot{\mathbf{O}}_{0r}, \tag{40}$$

where $\mathbf{M}_0$ is the mass matrix of moving platform; $\mathbf{f}$ is the resultant force and resultant moment array of the driving limbs acting on the moving platform. $\mathbf{F}_0$ is resultant force and resultant moment array of external force acting on the moving platform; $\ddot{\mathbf{O}}_{0r}$ is nominal acceleration array for moving platform of the mechanism. $\ddot{\mathbf{q}}_1 \cdots \ddot{\mathbf{q}}_6$ are the second-order derivative of $\mathbf{O}_0$. $\ddot{\mathbf{q}}_{cx}$, $\ddot{\mathbf{q}}_{cy}$, $\ddot{\mathbf{q}}_{cz}$ are the second-order derivative of the position vectors of the center of the moving platform with clearance. $\ddot{\boldsymbol{\alpha}}^*$, $\ddot{\boldsymbol{\beta}}^*$, $\ddot{\boldsymbol{\gamma}}^*$ are the second-order derivative of the Euler angle coordinates with clearance. $\mathbf{I}_{xx} \cdots \mathbf{I}_{zz}$ are the rotational inertia of the moving platform.

By (36), (37), and (40), the dynamic model of the parallel mechanism with joint clearance and flexible links is given by

$$\mathbf{M}\ddot{\mathbf{O}} + \mathbf{C}\dot{\mathbf{O}} + \mathbf{K}\mathbf{O} = \mathbf{Q}^*, \tag{41}$$

where $\mathbf{O} = \left[\mathbf{O}_{01}^T \ \mathbf{O}_{02}^T \ \mathbf{O}_{03}^T \ \mathbf{O}_{04}^T \ \mathbf{O}_{05}^T \ \mathbf{O}_0^T\right]^T$, $\mathbf{O}_0 = \left[\mathbf{q}_1 \ \mathbf{q}_2 \ \mathbf{q}_3 \ \mathbf{q}_4 \ \mathbf{q}_5 \ \mathbf{q}_6\right]^T$, $\mathbf{O}_{01} \cdots \mathbf{O}_{05}$ are the elastic displacements of driving limbs. $\mathbf{q}_1 \cdots \mathbf{q}_6$ are the elastic displacements of the moving platform caused by elastic deformation of driving limbs. $\mathbf{M}$ is total mass matrix of the mechanism, and $\mathbf{M} = \sum_{i=1}^{5} \mathbf{R}_i^T\mathbf{M}^i\mathbf{R}_i + \mathbf{R}_0^T\mathbf{M}_0\mathbf{R}_0$. $\mathbf{K}$ is the total stiffness matrix of the mechanism, $\mathbf{K} = \sum_{i=1}^{5} \mathbf{R}_i^T\mathbf{K}^i\mathbf{R}_i$. $\mathbf{Q}^*$ is the total generalized force matrix of the mechanism, $\mathbf{Q}^* = \sum_{i=1}^{5} \mathbf{R}_i^T\mathbf{Q}^{i*} + \mathbf{R}_0^T\mathbf{Q}_0$. $\mathbf{C}$ is the total damping matrix of the mechanism, and $\mathbf{C} = \sum_{i=1}^{5} \mathbf{R}_i^T\mathbf{C}^i\mathbf{R}_i + \lambda_1\mathbf{M} + \lambda_2\mathbf{K}$, $\lambda_1 = 2 \times 10^{-3}$, $\lambda_2 = 3 \times 10^{-4}$. $\mathbf{R}_i$ and $\mathbf{R}_0$ are the transfer matrix. $\mathbf{Q}_0 = \mathbf{M}_0\ddot{\mathbf{O}}_0$.

3.3. Solution of the Dynamic Model of the Parallel Mechanism with Joint Clearance and Flexible Links. The dynamic equation is a set of coupled nonlinear differential equations that can be solved by numerical integration method. In this paper, the Newmark algorithm and fourth-order Runge-Kutta method are used to solve the dynamic model. The calculation flow of dynamic model is shown in Figure 7. The detailed process is expressed as follows.

(1) Read in initial data displacements (q_c) and velocities ($\dot{q}_c$).

(2) Check for contact between the ball and socket. If the contact occurred, calculate the normal contact force ($\mathbf{F}_n$) and the tangential contact force ($\mathbf{F}_t$) according to continuous contact model proposed by Lankarani and Nikravesh and the modified Coulomb's friction model. Otherwise, the normal contact force and tangent contact force are zero.

(3) Compute the rigid body dynamic model of parallel mechanism with joint clearance by fourth-order Runge-Kutta method. The displacement ($\mathbf{q}_c$), velocities ($\dot{\mathbf{q}}_c$) of the moving platform, and the contact force ($\mathbf{F}_f$) on the first time step are obtained.

(4) Put the relevant quantities evaluated in process (3) into elastic dynamic model. Compute the elastic dynamic model by the Newmark algorithm. Elastic displacements ($\mathbf{O}_0$) and elastic velocities ($\dot{\mathbf{O}}_0$) of the moving platform are caused by elastic deformation of driving limbs can be obtained. Then the inertia force (**Fe**) and the moment of inertia (**Me**) of moving platform caused by the elastic deformation of driving limbs are solved.

(5) Update the system time variable. The influence of the inertia force (**Fe**) and the inertia moment (**Me**) of the elastic deformation are taken into account, and proceed with the whole process for the new steps.

(6) Repeat processes (1)–(5) for the next operation, and we can finally get the whole movement of the system.

4. Dynamic Behavior of Parallel Mechanism with Joint Clearance and Flexible Links

The distribution of the joints of 4-UPS-RPS spatial parallel mechanism is shown in Table 1. The parameters of 4-UPS-RPS spatial parallel mechanism are given in Table 2. The

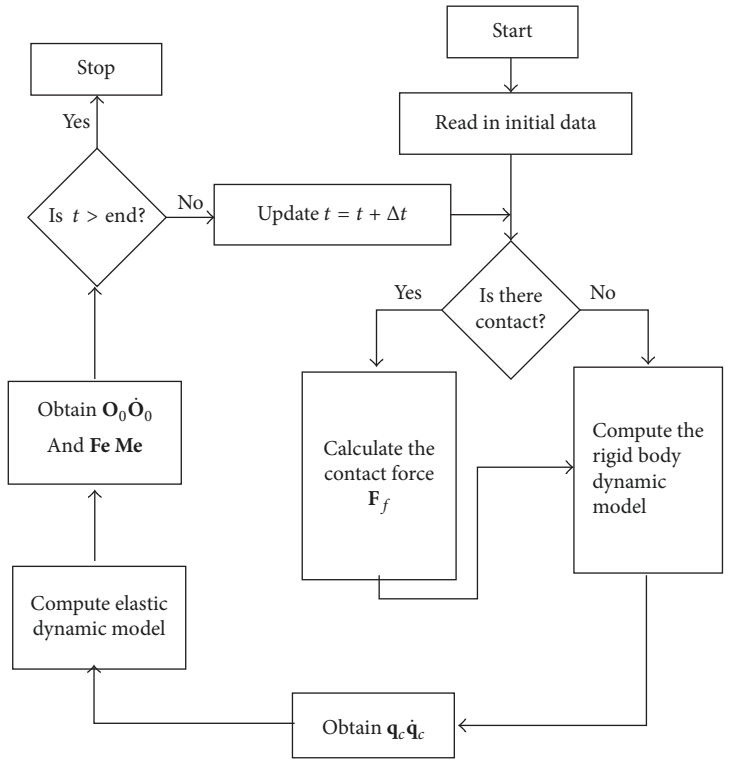

Figure 7: Calculation flow of dynamic model.

Table 1: The distribution of joints of 4-UPS-RPS parallel mechanism (m).

Hinge type	R	U_2	U_3	U_4	U_5	S_1	S_2	S_3	S_4	S_5
Distribution radius	0.71707	0.645	0.645	0.645	0.645	0.202	0.202	0.202	0.202	0.202
Distribution angle	0	$7\pi/4$	$5\pi/4$	$3\pi/4$	$\pi/4$	0	$8\pi/5$	$6\pi/5$	$4\pi/5$	$2\pi/5$

Table 2: The parameters of 4-UPS-RPS parallel mechanism.

Parameter	Value
Socket radius R_{S5}	0.0152 m
Clearance value	0.0002 m
The length of swing rod	0.760 m
The length of telescopic rod	0.840116 m
The cross section radius of telescopic rod	0.04 m
Integral tolerance	0.000001 s
Integral step d_t	0.001 s
The principal moment of inertia of the telescopic rod	$\mathbf{I}_x = 2.512 \times 10^{-7}$ kg·m^4 $\mathbf{I}_y = 1.256 \times 10^{-7}$ kg·m^4 $\mathbf{I}_z = 1.256 \times 10^{-7}$ kg·m^4
Ball radius R_{b5}	0.015 m
Recovery coefficient c_e	0.9
Friction coefficient c_f	0.05
Young' modulus E, E_{s5}, E_{b5}	200 Gpa
Shear elastic modulus G	80 Gpa
Poisson's ratio ν_{s5}, ν_{b5}	0.29
The mass of moving platform	36.28 kg
The moment of inertia of the moving platform	$\mathbf{I}_{xx} = 0.932$ kg·m^2 $\mathbf{I}_{yy} = 0.673$ kg·m^2 $\mathbf{I}_{zz} = 0.6816$ kg·m^2

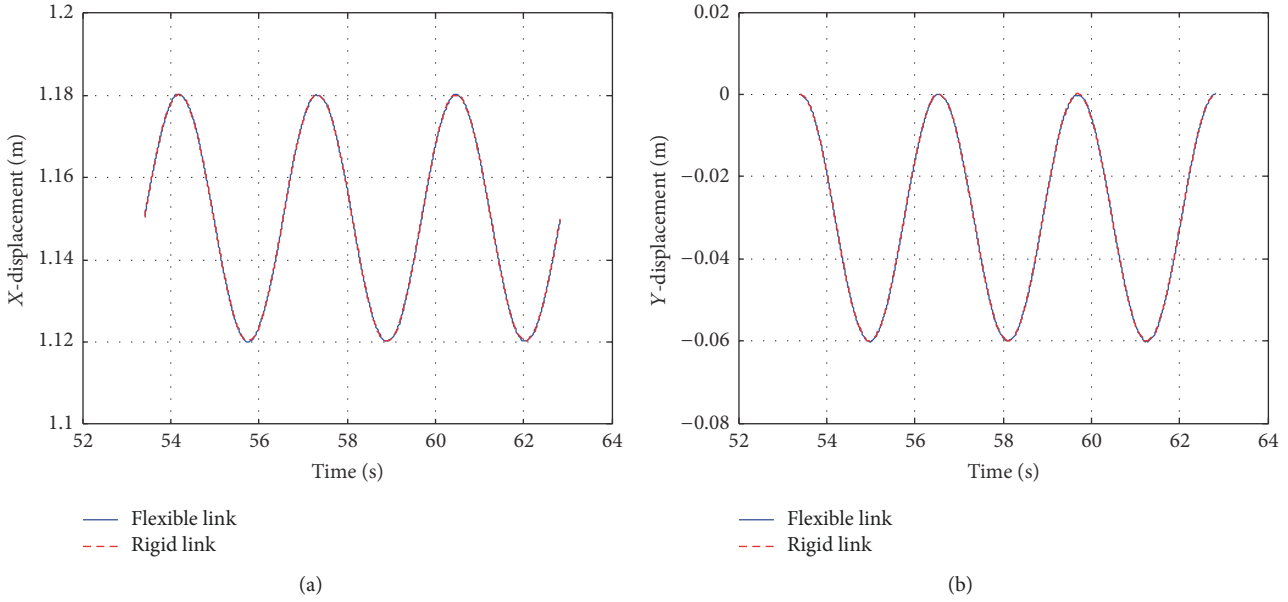

Figure 8: Displacement diagram of the moving platform: (a) displacement in X direction; (b) displacement in Y direction.

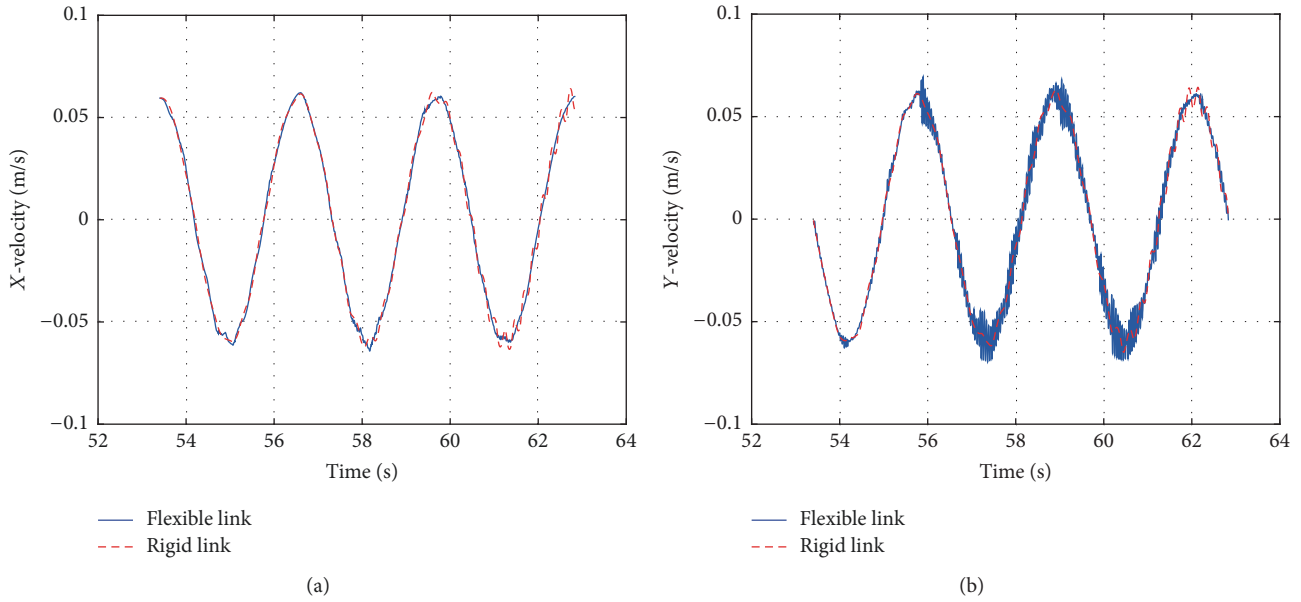

Figure 9: Velocity diagram of the moving platform: (a) velocity in X direction; (b) velocity in Y direction.

motion of the parallel mechanism is defined as follows (unit: s, m):

$$\begin{aligned} \mathbf{X} &= 1.15 + 0.03 \sin(2\mathbf{t}) \\ \mathbf{Y} &= -0.03 + 0.03 \cos(2\mathbf{t}) \\ \mathbf{Z} &= 0, \end{aligned} \tag{42}$$

where $\mathbf{X}$, $\mathbf{Y}$, $\mathbf{Z}$ are the position vectors of the center of the moving platform in the fixed coordinate system $\mathbf{O}_A - \mathbf{X}_A\mathbf{Y}_A\mathbf{Z}_A$.

4.1. The Effect of Flexible Links on Dynamic Response of Parallel Mechanism with Joint Clearance. In the movement process of 4-UPS-RPS spatial parallel mechanism, the influences of clearance on the dynamic response of the spatial parallel mechanism with flexible links and without flexible links are analyzed. The displacement diagram of the moving platform, the velocity diagram of the moving platform, the acceleration diagram of the moving platform, and the contact force diagram are shown in Figures 8, 9, 10, and 11, respectively.

As shown from Figures 8–11, the velocity curves and the acceleration curves of moving platform of the 4-UPS-RPS

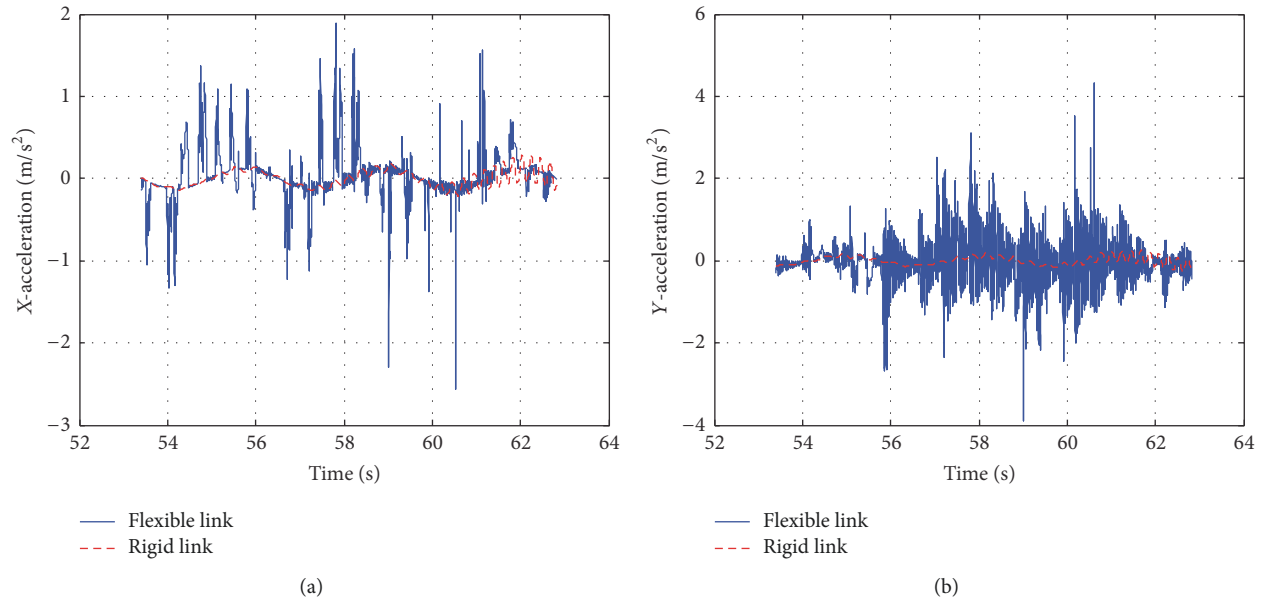

FIGURE 10: Acceleration diagram of the moving platform: (a) acceleration in X direction; (b) acceleration in Y direction.

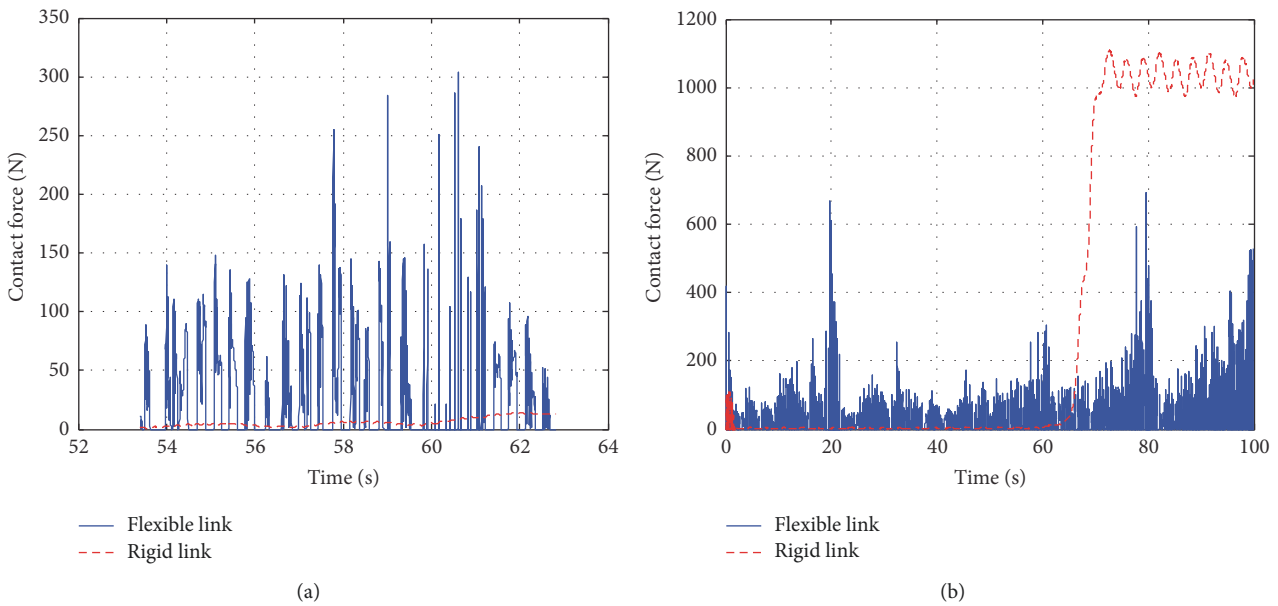

FIGURE 11: Contact force diagram: (a) within 52 s–64 s; (b) within 0 s–100 s.

parallel mechanism with flexible links and without flexible links all have fluctuation; the time points of the fluctuation of velocity and acceleration are consistent with the time points of collision; this shows that the collision is the reason of the fluctuation of velocity and acceleration. It can be seen from Figure 11 that flexible links has a serious impact on contact force response of parallel mechanism with joint clearance. The contact force intensively increases in a specific time duration compared to the case of rigid mechanism. When considering flexible links, the relative motion between the ball and the socket is always in the continuous impact and the contact force can intensify the deformation of the flexible links, besides, the elastic deformation of the flexible links could cause the contact force to increase; therefore the contact force fluctuates more widely. The appearance of this phenomenon may be related to the motion trajectory of the parallel mechanism and the size of clearance and so on. In general, the flexible components have a certain buffer effect on the compact force.

4.2. Chaos and Bifurcation of Parallel Mechanism with Joint Clearance and Flexible Links. As everyone knows parallel mechanism with joint clearance and flexible links is a typical nonlinear dynamical system, and chaotic phenomena and

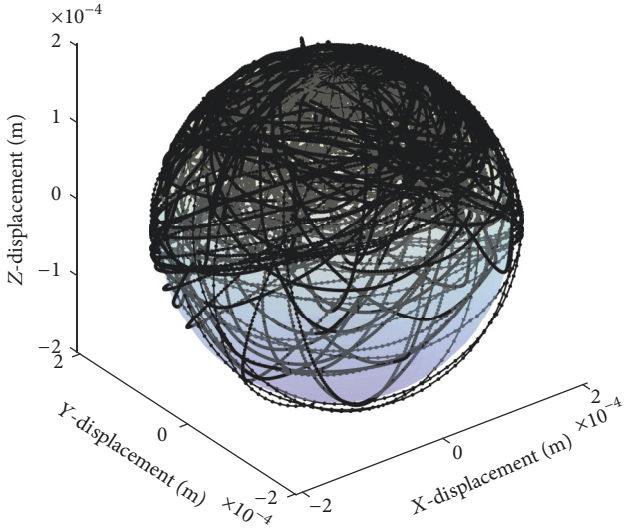

Figure 12: Trajectory of the ball center.

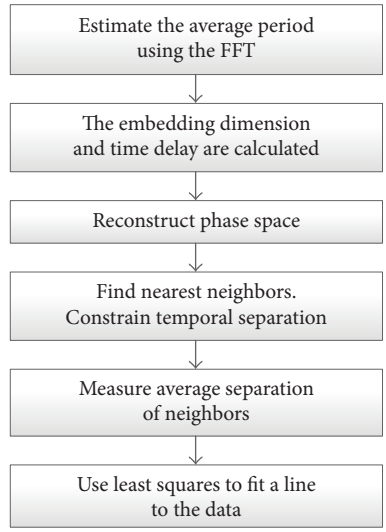

Figure 14: Flowchart of the small data sets method.

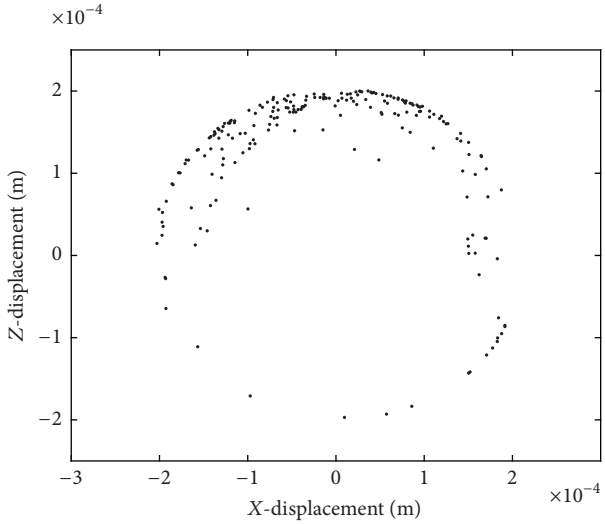

Figure 13: Poincare maps.

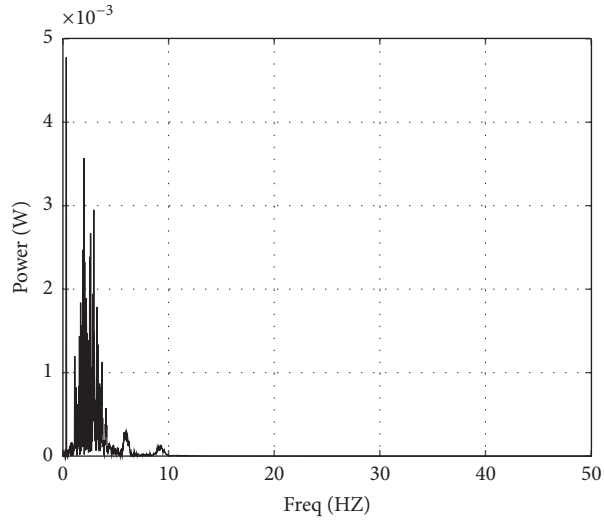

Figure 15: Power spectrum.

bifurcation must exist in the system; then chaotic and bifurcation should be analyzed. The trajectory of the center of ball is shown in Figure 12. From Figure 12, the trajectory of the ball center represented by solid line is messy and has no obvious periodic characteristics.

We can judge whether the system is chaotic or not by observing the intercept point on the Poincare map [22, 23]. When the Poincare map is only one fixed point or a small number of discrete points, the system is in periodic motion. When the Poincare map has a closed curve, the system is quasiperiodic motion. When the Poincare map is stretches of dense points and has a fractal structure, the system is in chaotic motion [24]. The Poincare maps of the system are shown in Figure 13. From Figure 13, the system is in chaos motion state.

The Lyapunov exponent is one of the important measurements to describe the dynamic characteristics of a system. The Lyapunov exponent is related to the nature of the phase space trajectory. In this paper, the small data sets method [25] is used to estimate the largest Lyapunov exponent; this method is reliable, fast, and easy to implement for small data sets. The flowchart of the small data sets method is shown in Figure 14.

As is well known, the average period P is estimated by means of FFT transform; namely, the average period can be obtained by reciprocal of the average frequency of power spectrum (see in Figure 15). Then the average period $P = 3$ can be obtained. From Figure 15, there are continuous peaks in the power spectrum, so the system is in chaos motion state. C-C algorithm [26] can be used to achieve embedding dimension m and time delay tau, respectively. After reconstructing the phase space and the largest Lyapunov exponent can be obtained by the least square method [27]. As shown in Figure 16, the largest Lyapunov exponent is 0.9537. It can be seen that chaos exists in the

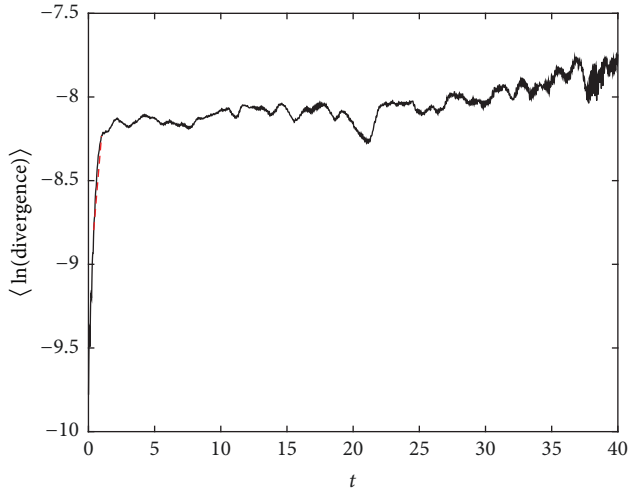

Figure 16: The largest Lyapunov exponents.

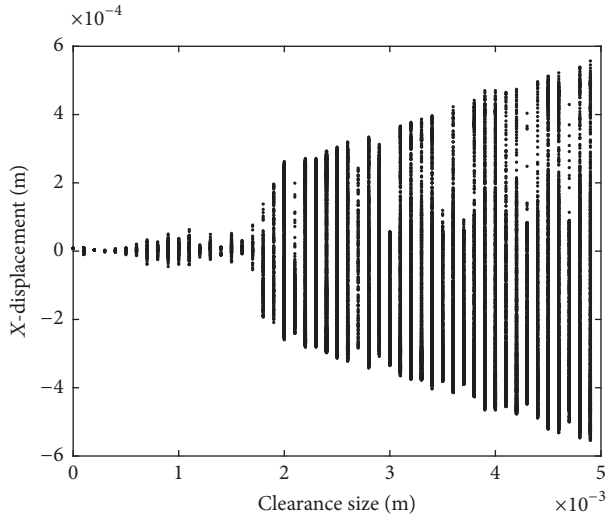

Figure 17: Bifurcation diagram.

mechanism. The system bifurcation diagram of displacement in x direction with clearance value using the Poincare section method is shown in Figure 17. From Figure 17, we can see joint clearance is one of the major factors of chaotic motion.

4.3. The Effect of Clearance Value on Dynamics Behaviors. It is well known that the joint clearance has a great influence on the dynamic characteristics of the mechanism with flexible links. The influence of the clearance value on the system stability is studied.

The Poincare maps of different clearances are shown in Figure 18. From Figure 18, with the increasing of values of joint clearance, the system transited from periodic motion to chaotic motion. When the joint clearance is 0.01 mm, there is an isolated point (see in Figure 18(a)) in Poincare map, so the system is in periodic motion state. When the joint clearance is 0.1 mm, there is a cycle (see in Figure 18(b)) in Poincare map, so the system is in almost periodic motion state. When the joint clearance is 0.25 mm or 0.5 mm, there are dense points with fractal structure (see in Figures 18(c) and 18(d)) in Poincare map, so the system is in chaotic motion state.

Trajectory of the ball center of different clearances and contact force of different clearances are shown in Figures 19 and 20, respectively. According to Figures 19(a) and 20(a), when the joint clearance is 0.01 mm, the trajectory of the ball center is outside the blue sphere (the blue sphere is made by taking the center of the socket as the center and the clearance value as the radius) and the values of contact force are positive; we can see that the type of relative motion is in continuous contact state. In this case, the system is stable. As shown in Figures 19(b) and 20(b), when the joint clearance is 0.1 mm, the trajectory of the ball center is concentrated on the top of the blue sphere, this part is more prone to wear. According to Figures 19(c), 20(c), 19(d), and 20(d), when the joint clearance is 0.25 mm or 0.5 mm, the types of relative motion include free flight motion, the contact

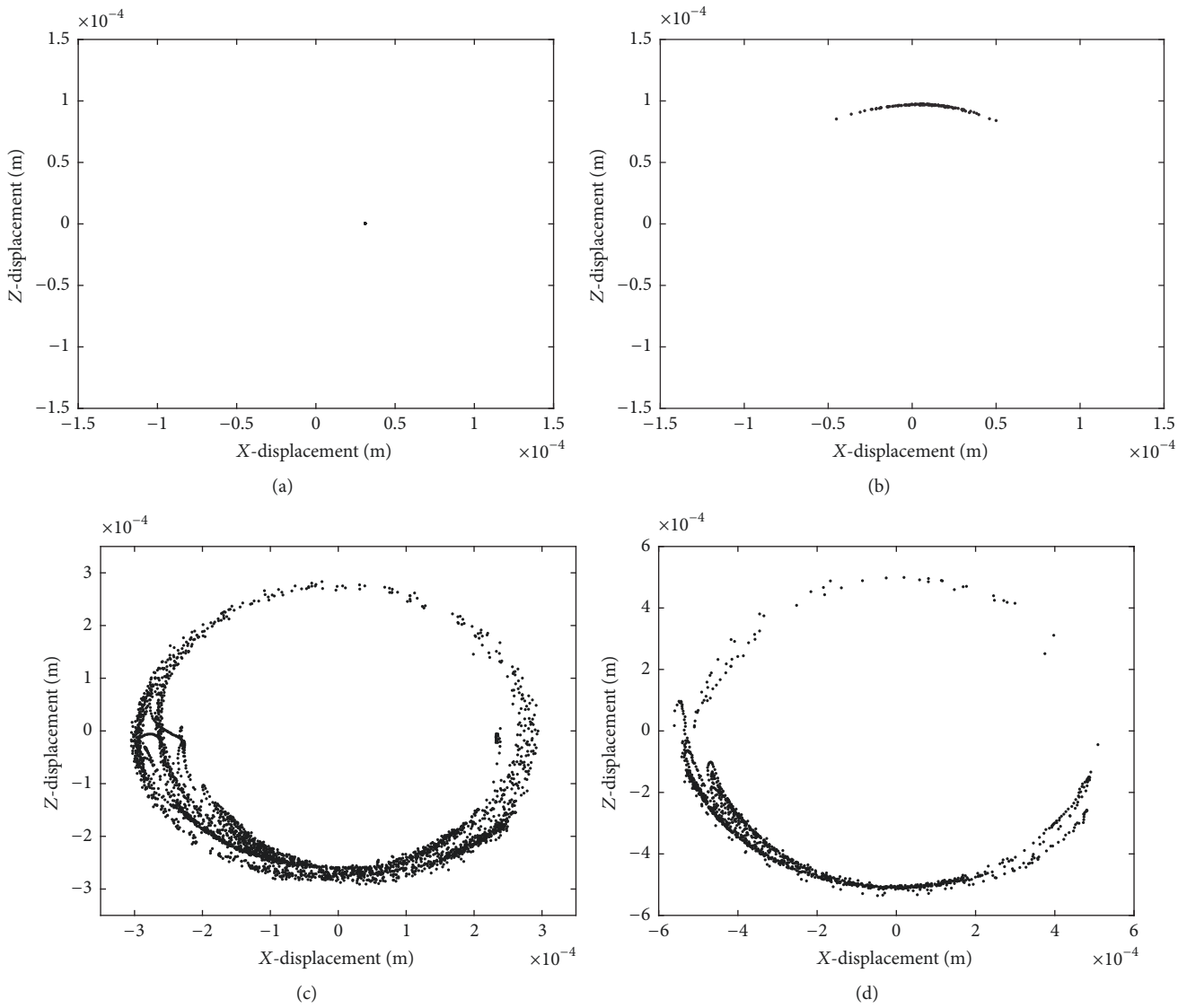

Figure 18: Poincare maps of different clearances: (a) $c = 0.01$ mm; (b) $c = 0.1$ mm; (c) $c = 0.25$ mm; (d) $c = 0.5$ mm.

motion, and impact. The contact frequency is obviously higher than the other cases; the system becomes unstable. As shown in Figure 20, the magnitude of the contact force value is not necessarily related to the relative motion, collision, and separation between elements of kinematic pairs and is the cause of chaos. When the elements of kinematic pairs are always in continuous contact state, the system is stable. Therefore, we can make the mechanism become relatively stable by controlling the type of relative motion.

5. Conclusion

This paper researches the dynamics behaviors of parallel mechanism with joint clearance and flexible links. The main conclusions are as follows: (i) a nonlinear dynamic model of 4-UPS-RPS spatial parallel mechanism considering clearance and flexible links is established by combining the KED analysis method and Lagrange method. (ii) The dynamic responses including collision force and motion characteristics of the moving platform for 4-UPS-RPS spatial parallel mechanism considering the spherical clearance and flexible links are analyzed. Chaos and bifurcation of 4-UPS-RPS spatial parallel mechanism with clearance and flexible links are analyzed by using trajectory of the ball center, Poincare maps, power spectrum, the largest Lyapunov exponent, and bifurcation diagram. The effects of different clearances on the dynamics behaviors of the parallel mechanism are studied. (iii) Joint clearance and flexible links, which all have a great influence on dynamic behaviors of 4-UPS-RPS spatial parallel mechanism, must be considered. This research provides a methodology for forecasting the dynamics behavior of parallel mechanisms with joint clearance and flexible links. (iv) The study of this paper shows that the chaos phenomena can be avoided by selecting suitable control parameter, and then the motion property of mechanism can be improved. The research can provide important theoretical basis for

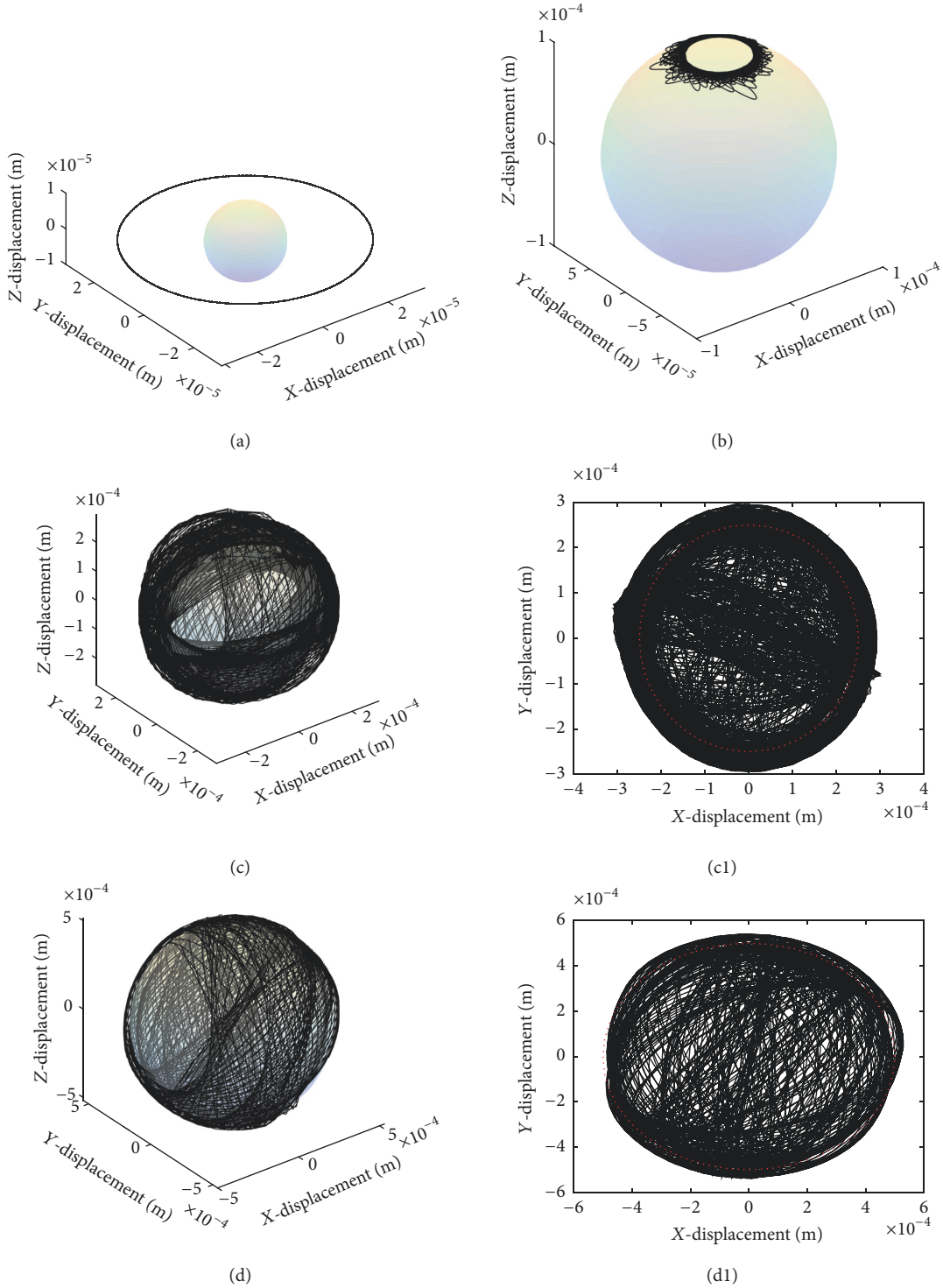

FIGURE 19: Trajectory of the ball center of different clearances: (a) $c = 0.01$ mm; (b) $c = 0.1$ mm; (c) $c = 0.25$ mm; (c1) a sectional view of Figure (c); (d) $c = 0.5$ mm; (d1) a sectional view of Figure (d).

the further research on the nonlinear characteristic of other spatial parallel mechanism.

Conflicts of Interest

The authors declare that they have no conflicts of interest.

Acknowledgments

This research is supported by the Natural Science Foundation of Shandong Province (Grant no. ZR2017MEE066), the Shandong Young Scientists Award Fund (Grant no. BS2012ZZ008), Taishan Scholarship Project of Shandong Province (no. tshw20130956).

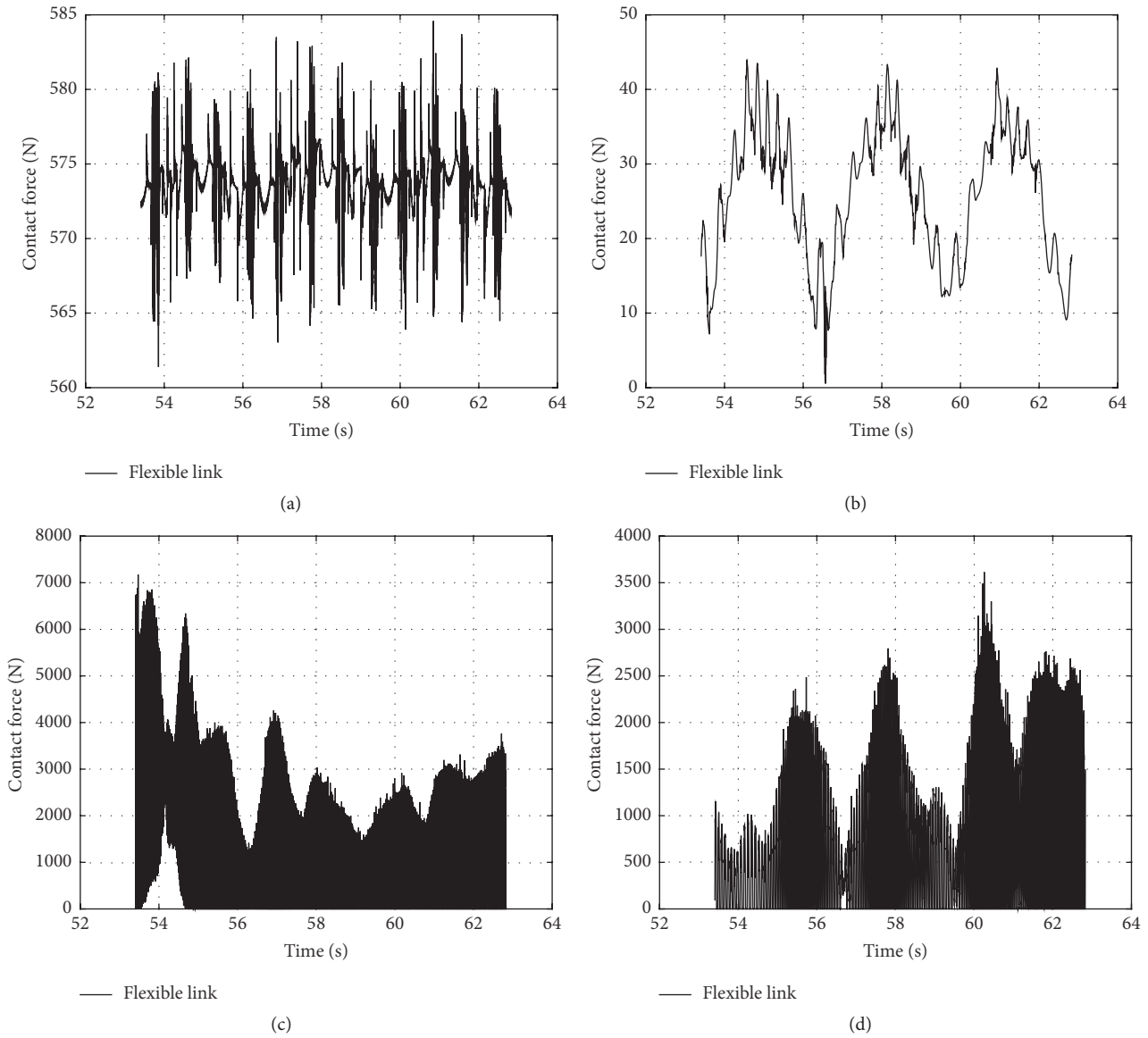

Figure 20: Contact force of different clearances: (a) $c = 0.01$ mm; (b) $c = 0.1$ mm; (c) $c = 0.25$ mm; (d) $c = 0.5$ mm.

References

[1] J. Kim, F. C. Park, S. J. Ryu et al., "Design and analysis of a redundantly actuated parallel mechanism for rapid machining," *IEEE Transactions on Robotics and Automation*, vol. 17, no. 4, pp. 423–434, 2001.

[2] Gao Lihua, Zheng Yaqing, and Mitrouchev Peter, "Dynamic model of wire-driven parallel suspension system based on ADAMS," *Journal of Shandong University of Science and Technology (Natural Science)*, vol. 32, no. 06, pp. 89–94, 2013.

[3] J. Liu, Y. Li, Y. Zhang, Q. Gao, and B. Zuo, "Dynamics and control of a parallel mechanism for active vibration isolation in space station," *Nonlinear Dynamics*, vol. 76, no. 3, pp. 1737–1751, 2014.

[4] Y. Yu, Z. Du, J. Yang, and Y. Li, "An experimental study on the dynamics of a 3-RRR flexible parallel robot," *IEEE Transactions on Robotics*, vol. 27, no. 5, pp. 992–997, 2011.

[5] H. M. Lankarani and P. E. Nikravesh, "A contact force model with hysteresis damping for impact analysis of multibody systems," *Journal of Mechanical Design*, vol. 112, no. 3, pp. 369–376, 1990.

[6] P. Flores and J. Ambrósio, "Revolute joints with clearance in multibody systems," *Computers & Structures*, vol. 82, no. 17-19, pp. 1359–1369, 2004.

[7] Z. F. Bai and Y. Zhao, "A hybrid contact force model of revolute joint with clearance for planar mechanical systems," *International Journal of Non-Linear Mechanics*, vol. 48, pp. 15–36, 2013.

[8] W. Bu, Z. Liu, J. Tan, and S. Gao, "Detachment avoidance of joint elements of a robotic manipulator with clearances based on trajectory planning," *Mechanism and Machine Theory*, vol. 45, no. 6, pp. 925–940, 2010.

[9] S. Dubowsky and T. N. Gardner, "Design and analysis of multilink flexible mechanisms with multiple clearance connections,"

ASME Journal of Engineering for Industry, vol. 99, pp. 88–96, 1977.

[10] E. Zheng and X. Zhou, "Modeling and simulation of flexible slider-crank mechanism with clearance for a closed high speed press system," *Mechanism and Machine Theory*, vol. 74, pp. 10–30, 2014.

[11] Jin Chunmei and Qiu Yang, "Dynamics research of mechanism with clearances based on FMD theory," *Chinese Journal of Mechanical Engineering*, vol. 37, no. 7, p. 18, 2001.

[12] X. C. Zhang, X. M. Zhang, and Z. Chen, "Dynamic analysis of a 3- R RR parallel mechanism with multiple clearance joints," *Mechanism & Machine Theory*, vol. 78, no. 78, pp. 105–115, 2014.

[13] S. Rahmanian and M. R. Ghazavi, "Bifurcation in planar slider-crank mechanism with revolute clearance joint," *Mechanism and Machine Theory*, vol. 91, no. 19, pp. 86–101, 2015.

[14] P. Flores and J. Ambrósio, "On the contact detection for contact-impact analysis in multibody systems," *Multibody System Dynamics*, vol. 24, no. 1, pp. 103–122, 2010.

[15] P. Flores, M. MacHado, M. T. Silva, and J. M. Martins, "On the continuous contact force models for soft materials in multibody dynamics," *Multibody System Dynamics*, vol. 25, no. 3, pp. 357–375, 2011.

[16] Y. Gonthier, J. McPhee, C. Lange, and J.-C. Piedbœuf, "A regularized contact model with asymmetric damping and dwell-time dependent friction," *Multibody System Dynamics*, vol. 11, no. 3, pp. 209–233, 2004.

[17] Qin Zhiying and Lu Qishao, "Analysis of impact process model based on restitution coefficient," *Journal of dynamics and control*, vol. 4, pp. 294–298, 2006.

[18] J. A. C. Ambrósio, "Impact of Rigid and Flexible Multibody Systems: Deformation Description and Contact Models," in *Virtual Nonlinear Multibody Systems*, vol. 103, pp. 57–81, 2003.

[19] G. Wang, H. Liu, P. Deng, K. Yin, and G. Zhang, "Dynamic Analysis of 4-SPS/CU Parallel Mechanism Considering Three-Dimensional Wear of Spherical Joint with Clearance," *Journal of Tribology*, vol. 139, no. 2, Article ID 021608, 2017.

[20] G.-X. Wang, H.-Z. Liu, and P.-S. Deng, "Dynamic modeling for a parallel mechanism considering spherical joint clearance," *Journal of Vibration and Shock*, vol. 33, no. 10, pp. 43–49, 2014.

[21] X. Chen, L. Wu, Y. Deng, and Q. Wang, "Dynamic response analysis and chaos identification of 4-UPS-UPU flexible spatial parallel mechanism," *Nonlinear Dynamics*, vol. 87, no. 4, pp. 2311–2324, 2017.

[22] G. Wen, H. Xu, and Z. Chen, "Anti-controlling quasi-periodic impact motion of an inertial impact shaker system," *Journal of Sound and Vibration*, vol. 329, no. 19, pp. 4040–4047, 2010.

[23] J. Xu and K. W. Chung, "Dynamics for a class of nonlinear systems with time delay," *Chaos Solitons & Fractals*, vol. 40, no. 1, pp. 28–49, 2009.

[24] Y.-J. Niu, X.-Y. Wang, F.-Z. Nian, and M.-J. Wang, "Dynamic analysis of a new chaotic system with fractional order and its generalized projective synchronization," *Chinese Physics B*, vol. 19, no. 12, Article ID 120507, pp. 97–104, 2010.

[25] M. T. Rosenstein, J. J. Collins, and C. J. De Luca, "A practical method for calculating largest Lyapunov exponents from small data sets," *Physica D: Nonlinear Phenomena*, vol. 65, no. 1-2, pp. 117–134, 1993.

[26] H. S. Kim, R. Eykholt, and J. D. Salas, "Nonlinear dynamics, delay times, and embedding windows," *Physica D: Nonlinear Phenomena*, vol. 127, no. 1-2, pp. 48–60, 1999.

[27] D.-C. Li, C.-C. Chang, and C.-W. Liu, "Using structure-based data transformation method to improve prediction accuracies for small data sets," *Decision Support Systems*, vol. 52, no. 3, pp. 748–756, 2012.